

# Hybrid Rocket Firing Experiments at Various Axial-Tangential Oxidizer Flow Rate Ratios

Kohei Ozawa<sup>1</sup> and Koki Kitagawa<sup>2</sup>

*Institute of Space and Astronautical Science, JAXA, Sagamihara, 252-5210, Japan*

Shigeru Aso<sup>3</sup>

*Kyushu University, Fukuoka, 819-0395, Japan*

and

Toru Shimada<sup>4</sup>

*Institute of Space and Astronautical Science, JAXA, Sagamihara, 252-5210, Japan*

**A bread board model (BBM) of an Altering-intensity Swirling Flow Type (A-SOFT) hybrid rocket engine was recently developed, and static firing experiments of the BBM were performed under various axial and tangential oxidizer mass flow rates. A-SOFTs are intended to control thrust at an optimal O/F and achieve a high baseline of regression rates with a fixed motor configuration. This is possible by controlling both the oxidizer mass flow rate and effective geometric swirl number. A simple model based on a continuous and monotonic function of oxidizer mass flux and effective geometric swirl number was able to accurately predict performance of experiments conducted on the A-SOFT BBM. The local fuel regression behavior in the axial direction of the A-SOFT BBM was shown to be like that of Swirling Oxidizer Flow Type (SOFT) hybrid rocket engine. Combustion efficiency was evaluated indirectly using equations for the efficiencies of thrust and specific impulse to eliminate errors due to local pressure shifts and the centrifugal force in swirling flows. In most cases, this indirect method compensated for the overestimations of  $c^*$  efficiency that resulted by directly using chamber pressure data.**

## Nomenclature

$a_0$  = regression rate coefficient

---

<sup>1</sup> Assistant Professor, Department of Mechanical and Control Engineering, Faculty of Engineering, Kyushu Institute of Technology, AIAA Member.

<sup>2</sup> Assistant Professor, Institute of Space and Astronautics, Japan Aerospace Exploration Agency, AIAA Member.

<sup>3</sup> Professor, Department of Aeronautics and Astronautics, Kyushu University, AIAA Senior Member.

<sup>4</sup> Professor, Institute of Space and Astronautics, Japan Aerospace Exploration Agency, AIAA Associate Fellow.

$a_n$	=	constants of polynomials for the approximation of thrust ( $n=1-5$ )
$A_t$	=	throat area [m <sup>2</sup> ]
$c^*$	=	characteristic velocity [m/s]
$C_F$	=	thrust coefficient [-]
$C_p$	=	specific heat at constant pressure [J/Kkg]
$D$	=	injector outlet diameter [m]
$dr$	=	radial length of tangential injector port [m]
$F$	=	thrust [N]
$G$	=	mass flux [kg/m <sup>2</sup> s]
$g_0$	=	gravitational acceleration at sea level [m/s <sup>2</sup> ]
$h_c$	=	ideal enthalpy per unit mass of productive gas [J/kg]
$h_{loss}$	=	enthalpy loss per unit mass due to heat loss in the sonic nozzle [J/kg]
$I$	=	momentum along axial direction [kgm/s <sup>2</sup> ]
$I_{sp}$	=	specific impulse [s]
$L$	=	fuel port length [m] or measurement interval [m]
$m$	=	mass [kg]
$M$	=	angular momentum [kgm <sup>2</sup> /s <sup>2</sup> ]
$\dot{m}$	=	mass flow rate [kg/s]
$N$	=	experimental run number [-]
$n_1, n_2$	=	regression rate exponents referring to sensitivity of oxidizer mass flux and effective geometric swirl number [-]
$n_i$	=	number of slits of tangential injector element [-]
$O/F$	=	oxidizer-to-fuel mass ratio [-]
$p$	=	pressure [Pa]
$\dot{r}$	=	regression rate [mm/s]
$r$	=	port radius [mm]
$R$	=	outer radius of solid fuel grain [m]
$S_e$	=	effective geometric swirl number [-]

$S_g$	=	geometric swirl number of tangential injector [-]
$t$	=	axial width of tangential injector port [mm] or time [s]
$\Delta$	=	error from the true value [-]
$\Delta t$	=	burn time [s]
$\Delta \tau$	=	sampling time interval of the data logging [s]
$x$	=	axial distance [m]
$\eta_{c^*}$	=	c* efficiency directly calculated from pressure ratio $p_c/p_{c_i}$ [-]
$\eta_{C_F}$	=	efficiency of thrust coefficient [-]
$\eta_{I_{sp}}$	=	$I_{sp}$ efficiency [-]
$\nu$	=	time constant of heat conduction equation [ $s^{-1}$ ]
$\rho$	=	density [ $kg/m^3$ ]
$\sigma$	=	standard deviation
$\tau$	=	time index by $\Delta \tau$ [-]

Subscripts:

0	=	start of burn
1	=	end of burn
$\infty$	=	converged
a	=	ambient
ax	=	axial direction
ave	=	axial-averaged
c	=	combustion chamber
i	=	ideal
n	=	nozzle
o	=	oxidizer
peak	=	peak of temperature
ref	=	referential
sf	=	solid fuel

t	=	throat
tan	=	tangential direction
vac	=	in vacuum
w	=	water
—	=	time-averaged or normalized value by ideal value

## I. Introduction

The controllability of thrust and oxidizer-to-fuel ratio (O/F) is crucial for maximizing  $\Delta V$ , and improving the flexibility of hybrid rocket propulsion systems for multipurpose flight operations by increasing  $c^*$  and reducing unburned propellant residuals. However, thrust and O/F are not independently controllable in conventional hybrid rocket propulsion systems because fuel regression rates are nonlinearly dependent on oxidizer mass flux. This behavior leads to shifts in the O/F, both during static and throttling operations. This phenomenon is called “mixture ratio shift [1]” or “O/F shift”.

Waidmann carried out a research on the feedback control of thrust at a constant O/F and pointed out that decreases in the total enthalpy per unit mass of product gases due to O/F shifts at deep throttle rates can be non-negligible [1]. To overcome this issue, he tried to automatically control mixture ratios using oxidizer injection from the pre- and post-combustion chamber. Feedback thrust control simulations were also demonstrated using instantaneous regression rate data, however it is not clear that feedback thrust control was demonstrated at a constant O/F in his work. Besides the low performances of hybrids in unplanned deep throttling, Ozawa and Shimada [2] challenged a conventional theory that O/F shifts in conventional hybrids cause negligible performance losses as long as the O/F shift is as expected in the planning process of the thrust curve. Their flight simulations showed that O/F shifts caused by the uncertainty of fuel regression behavior may lead to residuals of unused propellant which can reduce the performance in actual flight operations, even for sounding rockets of relatively low propellant mass fraction, as well as lower the  $c^*$ . These results suggest that the  $3\sigma$  limit of flight performance of conventional hybrids decreases due to the uncontrollability of O/F. Usuki and Shimada [3] compared flight performances between O/F controlled and uncontrolled hybrid rockets in a multipurpose hovering mission. The O/F controlled hybrid rockets hovered for a longer time over all the target altitudes than the O/F uncontrolled hybrids in this comparison. The latter two researches provided new perspectives on O/F shift and the potential benefits of O/F control in hybrids.

To control O/F shift independently of oxidizer mass flow rate or mass flux, the direct control of another regression rate parameter is required during the burn. In hybrid rockets using swirling oxidizer injection, this parameter is typically the geometric swirl number [4], defined as the angular momentum normalized by the injector outlet diameter and axial momentum. Henceforth, hybrid rockets using swirling oxidizer injection will be referred to as “Swirling Oxidizer Flow Type (SOFT)” hybrid rockets. This kind of injection technique was originally developed to increase regression rate. Knuth et al. [5] demonstrated that aft-end tangential oxidizer injection produces a strong swirl that increases fuel regression rates through improved heat transfer and turbulent mixing. Yuasa et al. [6] also independently showed that increases in regression rate resulting from the use of head-end tangential oxidizer injection could be closely correlated with the resulting geometric swirl number.

In this research, swirling oxidizer injection is intended to achieve both, higher regression rates and improved controllability of thrust and O/F. Figure 1 shows the concept of an O/F controlled hybrid rocket engine using axial and tangential oxidizer injections. The oxidizer feed line splits into separate axial and tangential branches each having a control valve. This configuration enables the control of oxidizer mass flow rate in each line separately. The combined oxidizer feeds of both lines become the mass flow rates and resulting swirl numbers at the head-end of the fuel port. The controllability of these two parameters enables throttling to be carried out at a constant O/F given that the geometry of the solid fuel grain and regression rate behavior are provided. This type of modified SOFT hybrid rocket will henceforth be referred to as an Altering-intensity SOFT (A-SOFT) hybrid rocket.

This article presents and discusses the results of static firing experiments conducted with the bread board model (BBM) type A-SOFTs. The purposes of this campaign are to demonstrate that A-SOFTs allow for fuel regression rate to be controlled by both the total oxidizer mass flux and axial to tangential mass flow ratio without altering the motor components, and to ensure that A-SOFTs have the attributes necessary for practical use. Simple methods for continuous thrust control should be characterized by continuous, monotonic and predictable fuel regression behavior that is a function of oxidizer mass flux and swirl number to avoid limit-cycle oscillations or local maxima and minima in the control range. Feedback control also requires to some extent the predictability of fuel regression behavior. As one of the first experimental researches on A-SOFTs, this study focuses on these three characteristics in static operation, though the practical operation of A-SOFTs requires knowledge on other characteristics such as hysteresis, uncertainties and transient behavior.

## II. Experimental Setup and Conditions

This section briefly presents the experimental setup, which is composed of a feed system, the engine tested and the control/sensing systems of the A-SOFT BBM. An overview of the experimental setup is shown in Fig. 2.

### A. Feed system

A schematic of the feed system is shown in Fig. 3. The main oxidizer feed line was divided into the two branches, both of which have choked orifices, for axial and tangential injections. Their cross-sectional area and discharge coefficients each give constant volumetric flow rates in static operation, and static axial to tangential oxidizer mass flow ratios if the pressure drop is assumed to be the same in both branches.

Table 1 shows the specifications of the choked orifices used in this set of the firing experiments. The efficiency of the orifices had been measured in the Akiruno Experiment Laboratory of ISAS, JAXA before this test campaign was carried out.

### B. Engine

A cross-section of the BBM A-SOFT engine is shown in Fig. 4. All the components are made of SUS304 stainless steel, except the nozzle, which is made of oxygen-free copper. The axial oxidizer flow was injected from the head end of the test piece, and the tangential flow was injected from two locations along the side wall of the cylindrical pre-combustion chamber. The dual injector consisting of these axial and tangential injector plates was placed in the head flange. Circumferential flow was injected from the 8 slits, and axial flow was injected from the 8 ports. The head part of the engine was equipped with the “dual injector assembly” consisting of an axial injector plate, with 8 ports, and a tangential injector plate with 8 slits and a geometric swirl number of 37.3, which is a normalized geometric parameter of tangential injectors to show swirl strength. A single port solid fuel grain made of polypropylene (PP) with a piece of heating wire for ignition was installed in the combustion chamber. The initial inner diameter is the same as that of the pre-chamber of the injector plate. A sonic nozzle with a throat diameter of 14 [mm] was used because the convergent-divergent nozzles optimal for the lowest chamber pressure experiments would have had area ratios of less than 2 and marginally improved performance. The nozzle had a pressure transducer port to measure chamber pressure to evaluate the engine performance and a thermocouple port to measure the temperature inside the nozzle for safety.

### C. Control & sensing systems

As is shown in Fig. 3, the apparatus was equipped with 5 pressure transducers, 5 thermocouples and a load-cell. Signals from the sensors were amplified by the amplifiers, converted from analogue to digital data by the AD converter, and the digital voltage data from the AD converter and their data calibrated into physical values were recorded on the laptop at sampling rates of 1[ms] and 100[ms], respectively, using the LabView 2013 SP1 [8].

The regulators and needle valves were manual adjusted to set the initial oxidizer feed pressure, purge gas pressure and flowrate of the oxidizer for ignition. The axial and tangential mass flow rates were calculated from the properties of the choked orifices, the pressure transducer measurements  $P_a$  and  $P_t$  and the thermocouple measurements  $T_a$  and  $T_t$ . The pressure transducer and thermocouple attached to the nozzle measured the chamber pressure and the temperature inside the structure of the nozzle, respectively.

The three pneumatic ball valves enabled manual and automatic control of the oxidizer and purge flows. The control program in LabView 2013 SP1 controlled the solenoid valves that operated the pneumatic valves and the igniter via the NI DAQ and the programmed relay unit. A voltage of 12 [V] was applied to the igniter, which was glued to the head-end of the grain such that it spanned across 240 degrees of the surface of the fuel port.

Major components of the test stand structure were provided by Kyushu University. Two flat springs enabled the upper frame to move axially from the base frame. Figure 5 shows a close-up of the thrust sensing system around the head-end of the upper moving frame. The thrust produced by the engine during firing displaces the moving frame against the load cell, and its signals are converted into digital voltage data. This data was recorded in the laptop by the amplifier and the NI DAQ. The play in the connection between the engine and the stand system accounts for a yaw directional misalignment in the thrust vector of around  $\pm 3$  degrees, causing less than a 0.14% decrease in the apparent measured thrust. The wires applying the preload to the engine have a misalignment of  $+0.15$  degree, leading to an error in the apparent measured thrust of less than  $+0.03$  %. The friction between the wire and the pulley leads to a slight increase of the apparent thrust.

In this experimental campaign, three video cameras were used: to observe the exhaust gases, a full view of the subsystems placed in the test room, and the switching of the pneumatic valves. The full view was monitored from the control room to observe the status of the subsystems in real time.

#### **D. Experimental conditions**

Table 2 and Fig. 6 summarize the experimental conditions and the pairs of the orifices used in each experiment. The maximum expected operational pressure (MEOP) and thrust over this experimental campaign were 1.65 [MPa] and 230 [N], respectively.

The experimental conditions were selected to allow for a two-variable parametric study of oxidizer mass flow rate (50%, 75% and 100% of the nominal value) and effective geometric swirl number (0, 11.0, 25.3, and 37.3). Varying the effective geometric swirl number was expected to lead to more fruitful results, such as the impact of effective geometric swirl number on propulsion performance, than varying the oxidizer mass flow rate. The previous study [7] had already presented a large number of fuel regression data with various conditions of oxidizer mass flux, and their fundamental mechanisms had already been revealed by Marxman's diffusion limited analysis [9].

Let us explain the definition of effective geometric swirl number, which is an extension of the geometric swirl number used in the field of swirling hybrids, adapted for the combined flows of the axial and swirl injectors used in this study. Geometric swirl number is defined as the normalized ideal angular momentum of the oxidizer flow by the radius of the flow path and the ideal axial momentum in the cross-section of the pre-chamber. We assume the injector design with the dimensions as shown in Fig. 4 b). We make the assumptions that the flow of oxidizer from both injectors is ideal and incompressible with uniform angular and axial momentum at any point within the pre-chamber, and that the ideal angular momentum and axial momentum of the two flows are conserved in the combined flow. These assumptions enable us to express the ideal angular momentum  $M$  and the ideal axial momentum  $I$  in the circular cross-section of the pre-chamber as

$$M = \frac{(D-dr)}{2} \frac{\dot{m}_{o_{tan}}^2}{n_i \rho_o dr t}, I = \frac{(\dot{m}_{o_{ax}} + \dot{m}_{o_{tan}})^2}{\rho_o \pi D^2 / 4} \quad (1)$$

where  $D$ ,  $dr$ ,  $t$  and  $n_i$  refer to the diameter of the pre-chamber, the width of the slits, the thickness of the slits and number of tangential injector elements, and  $\rho_o$ ,  $\dot{m}_{o_{ax}}$  and  $\dot{m}_{o_{tan}}$  refer to the density of the oxidizer, the mass flow rates of the oxidizer from the axial injector and tangential injector, respectively.

These expressions give an effective geometric swirl number  $S_e$  corresponding to the extension of geometric swirl number  $S_g$  for A-SOFTs as:

$$S_e = \frac{D(D-dr)}{n_i dr t} \frac{1}{(1 + \dot{m}_{o_{ax}} / \dot{m}_{o_{tan}})^2} = \frac{S_g}{(1 + \dot{m}_{o_{ax}} / \dot{m}_{o_{tan}})^2} \quad (2).$$

The results of  $S_e = S_g$  for  $\dot{m}_{o_{ax}} = 0$  and  $S_e \rightarrow 0$  for  $\dot{m}_{o_{tan}} \rightarrow 0$  in Eq. (2) reflect that  $S_e$  is an adaptation of  $S_g$  for A-SOFTs.

The operational thrust and the chamber pressure were predicted using a simple in-house performance computational program. In this program, the fuel regression behavior averaged over port length is modeled as

$$\dot{r}_{ave}(t) = a_0(1 + S_e(t)^2)^{n_2} G_o(t)^{n_1} \quad (3)$$

where  $(1 + S_e^2)^{n_2}$  refers to the sensitivity of the fuel regression to swirling oxidizer flows. This term was also used in the previous study [6] to evaluate SOFT firing test data. We define  $n_1$  and  $n_2$  as the oxidizer mass flux exponent and swirl number exponent, respectively. Due to the lack of useful data for correlating regression rate to geometric swirl number using PP, the constant exponent  $n_2$  was estimated based on previous firing test data using PMMA and GOX [6, 10]. The remaining constants  $a_0$  and  $n_1$  were based on previous firing test data using PP and GOX where  $S_g$  was 19.4 [7]. The operating conditions and performances of the engine were predicted assuming chemical equilibrium minimization of Gibbs Energy like the method used by the NASA-CEA program [11]. The product gases were assumed to consist of CH<sub>4</sub>, O<sub>2</sub>, CO<sub>2</sub>, H<sub>2</sub>O, CO, H, H<sub>2</sub>, OH and O. The choke condition at the nozzle throat gave the coupling problem between the chemical equilibrium state and the quasi-1D compressible flow model of the product gas. The performance predictions were carried out by solving this coupling problem assuming frozen flow over the nozzle.

### E. Time sequence

Figure 7 shows the time sequence of the firing experiments from runs #02 to #12. The burn time was 5 [s]. The terms “high” and “low” in Fig. 7 refer to “open and close” or “on and off”. Taking delays of the pneumatic valves into account, signals to the valves were sent earlier than their timed actions. The delay between the command signal and the action of the valves was about 0.2[s]. The ignition GOX valve is kept open until +0.1[s] to prevent a sudden drop in GOX supply during the transition to the main GOX supply. The igniter worked until +2.0[s] to ensure ignition of the fuel over the port. In run #01, the ignition GOX valve opened and the igniter turned on 2.0 [s] earlier than in the other cases.

### F. Data analyses

After the experimental campaign, the experimental data were analyzed to evaluate regression rate, O/F, thrust, and  $c^*$  efficiency. The regression rates averaged over the time and port length were based on the difference in the fuel mass before and after firing and the burn time. These values were used to calculate the ideal thrust,  $I_{sp}$  and thrust

coefficient, assuming 100%  $c^*$  efficiency. The experimental results of thrust and  $c^*$  efficiency were compared with these ideal performances for the fuel and oxidizer mass flow rates averaged over the burn time.

The averaged regression rate over the port and the time was calculated only from the experimental conditions and measured values. Let us define  $\overline{\dot{r}_{ave}}$  as regression rates averaged over the time and port length with the following equation as

$$\overline{\dot{r}_{ave}} = \frac{r_{1ave} - r_{0ave}}{\Delta t} = \sqrt{\frac{m_{sf_0} - m_{sf_1}}{m_{sf_0}} \frac{R_{ave}^2 - r_{0ave}^2}{\Delta t} + r_{0ave}^2 - r_{0ave}} \quad (4)$$

where  $r_0$ ,  $r_1$  and  $R$  refer to the port radius of the solid fuel grain before and after burn and the outer radius of the grain, respectively. The subscript ‘‘ave’’ refers to average over the time and the port length. The burn time  $\Delta t$  is defined as the duration of the test where the pressure remained over 75% of the peak pressure, after opening the main valve.

The three unknown constants in Eq. (3) were approximated with a least-squares method using the experimental data such as the initial and final port radii and the instantaneous oxidizer mass flow rates. Let us consider the time integration of Eq. (3) as

$$r_{1ave}^{2n_1+1} - r_{0ave}^{2n_1+1} = (1 + 2n_1) \frac{a_0}{\pi^{n_1}} \int_{t_0}^{t_1} (1 + S_e(t)^2)^{n_2} \dot{m}_o(t)^{n_1} dt \quad (5)$$

where  $r_{0ave}$  and  $r_{1ave}$  refer to the port radius evaluated by means of the mass loss method before and after a firing experiment. This equation includes the effect of port expansion with burn time. The right side of Eq. (5) can be approximated with numerical integration using time traces of the firing experiments as

$$r_{1ave}^{2n_1+1} - r_{0ave}^{2n_1+1} \sim (1 + 2n_1) \frac{a_0}{\pi^{n_1}} \sum_{\tau=\tau_0}^{\tau=\tau_1} \{1 + S_e^2(t = \tau\Delta\tau)\}^{n_2} \dot{m}_o^{n_1}(t = \tau\Delta\tau) \Delta\tau \quad (6)$$

where  $\Delta\tau$  and  $\tau$  refer to the sampling time interval of the data logging and the time index by  $\Delta\tau$ . To approximate the three constants  $a_0$ ,  $n_1$  and  $n_2$  over all the experiments, the following expression for the residual sum of squares of Eq. (6) is minimized:

$$\sum_N \left[ r_{1ave_N}^{2n_1+1} - r_{0ave_N}^{2n_1+1} - (1 + 2n_1) \frac{a_0}{\pi^{n_1}} \sum_{\tau=\tau_0}^{\tau=\tau_1} \{1 + S_e^2(t = \tau\Delta\tau)\}^{n_2} \dot{m}_o^{n_1}(t = \tau\Delta\tau) \Delta\tau \right]^2 \quad (7)$$

where the subscript  $N$  refers to the data in the  $N$ th experiment. The cases where the engine did not reach a steady burn were excluded from this approximation.

After the experimental campaign, efforts were also carried out to evaluate axial distributions of the regression rates averaged over the burn time using the burnt fuel grain. This evaluation requires axial distributions of the fuel port diameter after burns. In our research, a relation between mass and volume of water filling a fuel port was applied for

measurement of the port diameter. The measuring system shown in Fig. 8 was used to determine axial distributions of port diameter according to the following procedure:

- 1) The head-end of a fuel grain is sealed using a bottom cap with an O-ring and vertically mounted on a table.
- 2) A laser distance meter is mounted above the fuel grain and aimed (vertically) at the bottom of the grain.
- 3) A float (a colored plastic flat plate) is placed on the bottom cap to reflect light of the laser.
- 4) The mass of water to be poured is measured with a digital scale
- 5) The water is poured into the fuel port.
- 6) The increase in the water level is measured with the laser distance meter.
- 7) The procedure from 4) to 6) is repeated until the fuel port is filled with the water.

Figures 8 a) and b) show a view of the actual measurement of axial distribution of the fuel grain port and the schematic of the above procedure from 4) to 6), respectively. The mass of the water poured  $m$  has the following relation with the rise of the water level  $L$  at every measurement trial:

$$r_1 \Big|_{x=x_0+\frac{L}{2}} = \sqrt{\frac{m_w}{\pi\rho_w L}} \quad (8)$$

where  $\rho_w$  and  $r_1$  refer to density of the water and port diameter averaged over  $L$ , and  $x$  refers to the level before the pour. The results of the measurement gave the axial distributions of the regression rates as

$$\bar{r}(x) = \frac{r_1|x-r_{0ave}}{\Delta t} \quad (9).$$

We should note that accuracy of regression rates calculated using Eq. (9) is strongly affected by those of the digital scale and laser distance meter used for the measurement. Moreover, this method has a trade-off between the accuracy of the regression rates calculated and the rise of water level, which is equivalent to the length of the measurement interval, and the measurement instruments did not provide so high an accuracy. However, this method was practical for this research as the first step to acquire local regression data of A-SOFTs. Appendix A presents a discussion on the accuracy of the regression rates that can be expected using this measuring method.

The time-averaged O/Fs in the experimental campaign were compared with the following approximation based on the numerical time-integration of Eq. (3):

$$\overline{O/F} = \frac{\sum_{\tau=\tau_0}^{\tau=\tau_1} \{m_{oN}(\tau\Delta\tau)\Delta\tau\}}{2\pi\rho_s r L a_0 \sum_{\tau=\tau_0}^{\tau=\tau_1} \left\{ r_{aveN}(\tau\Delta\tau) (1+S_{eN}(\tau\Delta\tau)^2)^{n_2} \left( \frac{m_{oN}(\tau\Delta\tau)}{\pi r_{aveN}^2(\tau\Delta\tau)} \right)^{n_1} \Delta\tau \right\}} \quad (10).$$

where instantaneous axial and tangential oxidizer mass flow rates are required. The measured thrust was approximated with an empirical polynomial of the two operating variables  $\dot{m}_o$  and  $S_e$  as

$$F = a_1 + a_2\dot{m}_o + a_3S_e + a_4S_e^2 + a_5\dot{m}_oS_e \quad (11).$$

This monotonic and continuous polynomial to fit the predicted thrust in the planning of this experimental campaign, agreed well with the predicted thrust.

Evaluating the  $c^*$  efficiency of hybrid rocket engines using swirling flows poses a challenge. This is because the centrifugal force of the swirling flow forms a pressure distribution in the radial direction. The pressure transducers used to measure chamber pressure, which are typically placed on the cylindrical side wall of the combustion chamber, are often affected by this pressure distribution, overestimating  $c^*$  efficiency. Yuasa et al. [12] proposed a technique to indirectly evaluate  $c^*$  efficiency using  $I_{sp}$  efficiency and thrust coefficient to overcome this issue. We refer to the conventional method only requiring the chamber pressure measurement as the “direct method”; and designate the method proposed by Yuasa et al. as the “indirect method”. In this paper,  $c^*$  efficiency was evaluated using both methods for the sake of comparison.

The direct method refers to calculating real-to-ideal  $c^*$  ratio under the assumption that chamber pressure is uniform over the combustion chamber. The  $c^*$  efficiency  $\eta_{c^*}$  using the direct method is expressed as

$$\eta_{c^*} \equiv \frac{c^*}{c_i^*} = \frac{p_c A_t / \dot{m}}{(p_c A_t / \dot{m})_i} = \frac{p_c}{p_{c_i}} \quad (12)$$

where  $A_t$  and  $\dot{m}$  refer to cross-sectional area of the nozzle throat and propellant mass flow rate under the assumption that their ideal values are equal to those measured in the experiments. In contrast, the indirect method determines  $c^*$  efficiency using the efficiencies of thrust coefficient and specific impulse to compensate for the apparent pressure increase due to centrifugal force in swirling flows. Under the same assumptions used in the direct method that the measured values of  $A_t$  and  $\dot{m}$  are equal to the ideal values, the specific impulse efficiency has the following relation with thrust coefficient and  $c^*$ :

$$\eta_{I_{sp}} = \frac{I_{sp}}{I_{sp_i}} = \frac{F/\dot{m}}{F_i/\dot{m}_i} = \frac{c^* C_F}{c_i^* C_{F_i}} = \frac{p_c C_F}{p_{c_i} C_{F_i}} = \eta_{c^*} \eta_{C_F} \quad (13).$$

This relation suggests that  $c^*$  efficiency  $\eta_{c^*}$  can be evaluated by  $\eta_{I_{sp}}/\eta_{C_F}$ . Yuasa et al. [12] showed that this method is robust against the apparent pressure increase with optimal expansion nozzle, assuming a constant  $\eta_{C_F}$  of 0.98 and a negligible heat loss. A review article by AGARD [13] has already shown that viscosity and real-gas effects slightly affect the efficiencies  $\eta_{I_{sp}}$ ,  $\eta_{c^*}$  and  $\eta_{C_F}$  in sonic nozzles over the operational range of this experimental campaign.

However, the copper nozzle with a large heat conduction coefficient requires an evaluation for the heat loss to assume a constant  $\eta_{cF}$  over the test campaign. The heat loss of the nozzle flow is discussed using time traces of nozzle temperature in the following section.

### III. Results & Discussion

#### A. Overview of the Time Traces of the Firing experiments

The functional tests and the experimental campaign were performed between Jan. 4th, 2016 and Jan. 29th, 2016 at Kyushu University.

During the experimental campaign, the engine sometimes did not reach a steady burn. In run #01, an ignition delay occurred because the solid fuel was not heated enough for the short heating time. This problem was solved by extending the heating time. However, despite a successful ignition, the engine did not reach a steady burn due to the position of the heating wire. In this experimental campaign, a piece of heating wire is glued along 2/3 of the circumference at the head-end of the grain, and so the heating of the remaining 1/3 circumference of the fuel port can be delayed longer, especially for axial injection tests. In fact, both runs #01 and #11 were axial injection tests. This problem will be solved by mounting assistant fuel such as steel wool in the future experiences. In runs #08 and #09, the ignition failed probably due to poor adhesion of the heating wire and a low battery power. All other test engines were successfully ignited and achieved steady burns.

Figure 9 shows the time traces of chamber pressure, thrust, oxidizer mass flow rates and effective geometric swirl number in run #04. In this test, the ignition sequence started from -4.4 [s] at a small flow rate of GOX. Once the main GOX valve opened at 0.0 [s], the engine smoothly transitioned to a steady burn over a transient state between 0.0 [s] and +1.1 [s]. The combustion was stable and the chamber pressure followed the total oxidizer mass flow rate.

Figure 10 shows some pictures of the static firing experiments in 100% nominal oxidizer flowrate. In run #04, droplets of the fuel were observed in the exhaust gas exiting the nozzle. The number of fuel droplets decreased in run #06, which had a larger  $S_e$ , as is shown in the Fig. 10 b) even though the fuel regression rate increased. These observations suggest that strong swirling flow improves  $c^*$  efficiency.

#### B. Averaged fuel regression rates

Table. 3 summarizes the results of the firing experiments. The least square minimization of Eq. (7) with the time traces of the results gave the constants  $(a_0, n_1, n_2) = (2.557 \times 10^{-5}, 0.651, 0.0987)$  for Eq. (3) in the SI system of units. Figure 11 compares the actual and approximated fuel regression, which were evaluated as

$$\begin{cases} \Delta r_{1\text{ave}} = \frac{r_{1\text{ave}} - r_{0\text{ave}} - a_0 \sum_{\tau=\tau_0}^{\tau=\tau_1} \left\{ (1 + S_e^2(\tau\Delta\tau))^{n_2} \left( \frac{m_o(\tau\Delta\tau)}{\pi r_{\text{ave}}^2(\tau\Delta\tau)} \right)^{n_1} \Delta\tau \right\}}{r_{1\text{ave}} - r_{0\text{ave}}} \\ r_{\text{ave}}((\tau + 1)\Delta\tau) = r_{\text{ave}}(\tau\Delta\tau) + a_0 (1 + S_e^2(\tau\Delta\tau))^{n_2} \left( \frac{m_o(\tau\Delta\tau)}{\pi r_{\text{ave}}^2(\tau\Delta\tau)} \right)^{n_1} \Delta\tau \end{cases} \quad (14).$$

Figure 12 shows a comparison of the regression rates averaged over burn time and port length  $\bar{r}_{\text{ave}}$  with the following prediction of  $\bar{r}_{\text{ave}}$  using the measured time traces of the oxidizer mass flow rates:

$$\bar{r}_{\text{ave}} = \frac{a_0 \sum_{\tau=\tau_0}^{\tau=\tau_1} \left\{ (1 + S_e^2(\tau\Delta\tau))^{n_2} \left( \frac{m_o(\tau\Delta\tau)}{\pi r_{\text{ave}}^2(\tau\Delta\tau)} \right)^{n_1} \Delta\tau \right\}}{\Delta t} \quad (15).$$

This approximation had good agreement with the experimental results. The monotonic and continuous function Eq. (3) approximated this behavior with high accuracy. The standard deviation of the approximation was  $6.0 \times 10^{-2}$  [mm] which corresponds to just 2.7% of the averaged fuel regression over the experimental campaign. This good agreement suggests monotonic and continuous dependence on both oxidizer mass flux and effective geometric swirl number, and demonstrates the ease of prediction of the fuel regression behavior of A-SOFTs using the two operating variables. These favorable characteristics will enable a simple feedback thrust control at a constant O/F.

However, to confirm this favorable behavior of A-SOFTs, more fuel regression data should be collected for low effective geometric swirl numbers, as well as for the axial injection case. Fuel regression behavior for weak swirl numbers seems to be especially important because Pucci [14] reported a higher risk of unstable combustion for weak swirl numbers under axial injection than for strong swirl injection, and Eq. (3) suggests that fuel regression behavior has a large sensitivity to  $S_e$  in low  $S_e$ . Fuel regression behavior for axial injection is also required because two of the three axial injection runs in this campaign did not achieve a steady burn.

In Fig. 13, experimentally determined regression rates from this research are compared with those of SOFTs with  $S_g = 19.4$  using PP and GOX reported in Ref. [7]. The data from Ref. [7] was collected from various scales of engines. Length and initial port diameter of the fuel grains ranged from 0.15 to 1.0 [m] and 40 to 56 [mm], respectively. The regression rates of the A-SOFT BBM with  $S_e = 25.3$  and  $S_e = 37.3$  were buried in the scatter of the reference data. Conversely, the regression rates for  $S_e = 11.0$  and  $S_e = 0.0$  were apart from those of the SOFTs. The reason for lower regression rates in the A-SOFT BBM for large  $S_e$  is attributed partly to the design of the tangential injector. The

tangential injector used for this experimental campaign was intended to give a geometric swirl number larger than that of the SOFTs. The larger circumferential velocity given by the tangential injector should cause a larger loss of angular momentum due to viscosity and turbulence, mainly in the forced vortex region and in the boundary layer near the wall. The swirl number exponent  $n_2$  of 0.0987 was also lower than that of 0.156 for SOFTs using PMMA and GOX. The low exponent in A-SOFTs compared to that in SOFTs using PMMA was possibly due to the chemical composition of PP as well. The stoichiometric O/F of PP and GOX is higher than that of PMMA and GOX, and this characteristic suggests that swirling flows in the combustion chamber are heated with a smaller mass of PP than of PMMA. In swirling hybrids, increasing the circumferential oxidizer flow enhances heat transfer to the fuel, and thus improves fuel regression rates. This effect corresponds to an increase in eddy viscosity in the boundary layer combustion in swirling hybrids, and the improved fuel regression and combustion lead to an increase in local axial momentum, ultimately resulting in a decrease in local swirl number [18]. Because a given volume of PP can increase the temperature of swirling flow more than the same volume of PMMA, PP should decrease the local swirl number and local regression rates within a shorter port length than PMMA. This mechanism can explain the smaller sensitivity of regression rates of PP to effective geometric swirl number.

### **C. Local regression rate behavior**

Figure 14 summarizes the local regression rates with their error bars in all the successful cases at each effective geometric swirl number. The plots in the experimental cases were summarized into four graphs for different effective geometric swirl numbers. Small intervals in axial position caused large error bars in the head-end region. A laser distance meter with better accuracy will solve this problem. The port diameter measurements in the head-end region were carried out several times. The diameters in the head-end region were slightly different each time possibly because bubbles remained on the spiral-shape surface of the fuel ports and prevented the fuel from being filled with the water.

Figure 14 also shows that the regression rates at the head-end of the fuel are 2 to 3 times larger than those averaged over the length for all the cases including axial injection. This uneven regression behavior is a fundamental problem common to axial and swirling injection hybrid rocket engines, leading to a significant residual of unburned propellants and a large performance loss. Currently, we have two ideas for how to overcome this challenge. The first idea is to use a fuel grain with a smaller regression rate in the head-end region than that in the middle and tail-end regions. This type of grain may be made up of two kinds of solid fuels to compensate for uneven regression in the head-end region. The other idea is to thicken the insulation in the head end region. Generally, the insulating materials used between the

motor and the solid propellant in solid rocket motors have quite small regression rates. Such insulation, which is used to protect the motor against high temperature combustion gas, is also practical for hybrid rocket propulsion systems, for example between the solid fuel and the motor case. Thickening the insulation in the head-end region should prevent the motor case from being exposed from the heat and high temperature gas with minimal increase in structural mass.

The local regression rates increased with increasing oxidizer mass flux for  $S_e=25.3$  and  $37.3$  as is shown in Figs. 14c and d. For  $S_e=11.0$ , the regression rates fluctuated in the region between port lengths of 90 and 110 [mm], and sometimes the runs for lower oxidizer mass flux had larger local regression rates than those for the largest oxidizer mass flux, though the error bars overlap one another. Small steps made in the manufacturing process of the grains can cause these fluctuations. The fuel grains used in this experimental campaign were manufactured in-house by drilling from both head- and tail-ends of the grain to overcome the limited span of the drill, which sometimes leads to small steps or ridges in the fuel grains.

Instead of large errors and variances of local regression rates, Fig. 15 shows that the measurements using the laser distance meter gave almost the same regression rates averaged over port length and burn time as those calculated from the mass and the initial geometries of the fuel grains. This is mainly because the uncertainties of the laser distance meter and digital scale become relatively small with the increasing mass and level of the water measured.

Figure 16 compares the axial distributions of regression rates in the 100% oxidizer throttle cases. The error bars of the measured regression rates were omitted for better readability. One interesting tendency observed in the regression rates was a large sensitivity to swirling number in the head-end region. For example, the regression rates increased by 2.3 times in the head-end region for an increase from  $S_e=0.0$  and  $25.3$ , whereas the regression rates increase only 1.7 in the middle and tail-end region. Any significant dependency on axial position should be considered in the design of fuel grains or thermal designs of the combustion chamber because large differences in the regression rate across port length can present problems in spending the solid fuel without residuals or in estimating and controlling fuel mass flow rates for throttling. Similar characteristics were seen also for  $S_e=37.3$  without axial oxidizer injection, which is equivalent to a SOFT of  $S_g=37.3$ . This tendency was also mentioned in parametric data analyses of SOFTs by Shiraishi et al. [17]. They pointed out that SOFTs have different fuel regression rate behavior in the head-end region than in other regions. Ozawa et al. [15] theoretically showed that a large increase in the regression rates in the head-end region due to the large geometric swirl number enhances combustion in this region, resulting in the following three effects: a large increase in the axial velocity of the product gas, a drastic decrease in the local swirl number, and a rapid growth

of the boundary layer. Furthermore, this quickly causes a moderate increase in regression rates downstream. In this respect, the results suggest that the A-SOFTs BBM have a similar mechanism and tendency of local regression rate behavior to SOFTs.

Figure 17 compares the axial distributions of regression rates of the A-SOFTs in this study with those of the SOFTs with  $S_g = 19.4$  in Ref. [7]. In this comparison, we selected tests conducted under similar operating conditions. The results of runs #12 and #07 with  $S_e = 25.3$  at the oxidizer mass flux of 42.1 and 51.7 [kg/m<sup>2</sup>s] in the averaged diameter method [16] were compared with those of the SOFTs at the oxidizer mass flux of 43.6 and 55.0 [kg/m<sup>2</sup>s], respectively. The reference paper says that the SOFT engine had an initial port diameter ranging between 40 and 48 [mm] and a grain length of 600 [mm]. In both the comparisons, the A-SOFT BBM resulted in smaller regression rates than the SOFTs over the whole length of fuel except for in the head-end region (less than 20 [mm]). As is shown in Fig. 13, there are some cases where the SOFTs had lower regression rates than those of the A-SOFT BBM with  $S_e = 25.3$ . The low regression rates of the A-SOFT BBM suggest that the dual injector with  $S_e = 25.3$  provides less angular momentum than a tangential injector with  $S_g = 25.3$  due to low efficiency of the tangential injector with  $S_g = 37.3$ . However, both the SOFTs and the A-SOFT BBM have a similar trend of decreasing local regression rate with increasing position downstream. This tendency suggests that both the axial and tangential oxidizer flows are combined well shortly after injection, and possibly that much research previously conducted using the SOFTs is also useful for A-SOFTs under the range operating conditions tested. The SOFTs did not apparently have the trend of decreasing regression rates in the tail-end region that was observed in the A-SOFTs from 91 to 100% of the grain length. However, a similar trend was also found in the SOFTs from 83 to 100 % of the grain length. An explanation for the phenomena is that the flame separated from the fuel port in the tail-end of the port due to the convergent part of the nozzle. The A-SOFT BBM has a steep convergent section near the interface with the fuel port which may separate the diffusion flame from the fuel port. Visualization experiments of SOFTs in Ref. [18] provided a series of results supporting this explanation. More detailed investigations in the tail-end region require firing experiments using an aft-combustion chamber or without a nozzle. As a result, despite small differences, this experimental campaign showed that the A-SOFT BBM has quite similar characteristics of fuel regression rates to those of the SOFTs in many aspects.

#### **D. O/F and thrust**

Figure 18 shows a comparison of the time-averaged O/Fs at the throttle settings of 50, 75 and 100% of the nominal value with the approximation using Eq. (10). The time-averaged O/Fs monotonically decreased with increasing  $S_e$  and increased with increasing  $m_o$ . This approximation fit to the experimental results with a determination coefficient of 0.996. Such good agreement suggests that the time-averaged O/F of the A-SOFT BBM can be predicted with good accuracy as well as the regression rate behavior.

The ability to easily predict O/Fs is beneficial for thrust feedback control at a constant O/F, because this involves the prediction of the instantaneous O/F. Under the assumption that local regression behavior has a uniform distribution across the port length, for example, the following prediction model also satisfies the requirement for thrust control:

$$\begin{cases} O/F = \frac{(1+S_e(t)^2)^{-n_2} m_o^{1-n_1(t)} r_{ave}^{2n_1-1}(t)}{2\rho_{sf} L a_0 \pi^{1-n_1}} \\ r_{ave}(t) = r_{ave}(0) + \int_0^t \dot{r}_{ave}(t) dt \end{cases} \quad (16).$$

However, A-SOFTs have large differences in regression rates between the head-end and the other regions. This means that real-time measurement techniques of the solid fuel web thickness are necessary to predict local oxidizer mass flux and regression rates and reduce the accumulation of time-integration errors in the predictions.

Figure 19 shows a comparison among the predicted, measured and approximated thrust, the latter of which was approximated by the polynomial Eq. (11). The multiple regression analysis using Eq. (11) resulted in good approximations for all the successful experimental cases, and the approximated coefficients of Eq. (11) resulted in  $a_n (n = 1, 2, \dots, 5) = (24.7, 1.21 \times 10^3, -3.38 \times 10^{-2}, -1.85 \times 10^{-2}, 25.7)$  in SI units with the determination coefficient of 0.973. The approximated thrust data were within  $\pm 1\sigma$  of the thrust measurement errors. The lower accuracy of thrust than that of the O/F can be attributed to the dependence of other performance factors such as  $c^*$  efficiency on the operating variables not modelled in the prediction. The Isp efficiency ranged from 0.7 to 0.8 in all the successful experiments. Such low performance was also observed in other experiments using PP [12], possibly because the pyrolyzed species have different characteristics such as viscosity and chemical reaction rates, leading to a different mixing process with the oxidizer from those of other fuels which result in higher  $c^*$  efficiency, such as PMMA.

### E. Evaluation of $c^*$ efficiency

The  $c^*$  efficiencies of the A-SOFT BBM in this study were evaluated using two methods, the direct method often used under the assumption of a uniform chamber pressure and the indirect method proposed by Yuasa et al.[12] The

indirect method applies the relation among Isp efficiency, efficiency of thrust coefficient, and  $c^*$  efficiency. However, the apparent chamber pressure shift of swirling hybrids complicates the estimation of the thrust coefficient because determining the thrust coefficient requires a chamber pressure representative of the combustion process and the actual specific heat ratio. For this reason, in the following analysis, the thrust coefficient  $\eta_{CF}$  for run #02 with axial injection was used for the analyses of all the successful experiments. This substitution requires there to be relatively small dependence of  $\eta_{CF}$  on the operating conditions over the entire experimental campaign. Even considering real gas effects and viscosity, the  $\eta_{CF}$  of sonic nozzles is expected to shift at most by  $\pm 0.1\%$  between chamber pressures of 0.9 and 1.2 [MPa] and between throat Reynolds number  $Re_{throat}$  of  $1.34 \times 10^5$  and  $1.53 \times 10^5$ , according to Ref. [13]. Moreover, this survey says that  $\eta_{CF}$  is less sensitive to chamber pressure with increasing temperature. However, this survey assumes a chamber temperature of around 300 [K], and so we should consider the large heat losses in the nozzle in our experiments.

In this study, heat losses in the sonic nozzle were approximated from the time traces of nozzle temperature converging after the burn by applying the basic knowledge that the one-dimensional heat conduction equation has an exponential eigenfunction converging to thermal equilibrium [19]. The convergence nozzle temperature was given by the approximation of the time traces of nozzle temperature with the following fitting equation:

$$T = (T_{peak} - T_{\infty}) \exp\{-\nu(t - t_{peak})\} + T_{\infty} \quad (17)$$

$T_{peak}$  and  $t_{peak}$  refer to the maximum temperature of the thermocouple in the nozzle over the run and the time corresponding to that temperature, respectively. The other constant variables  $T_{\infty}$  and  $\nu$  refer to the steady-state temperature for when  $t \rightarrow \infty$  and a time constant, respectively. This approximation assumes that heat transfer rate from the bulk oxygen-free copper to the purged gas flow, ambient air, and the structure of the combustion chamber is far much lower than the heat conduction rate in oxygen-free copper. Eq. (17) fit all the time traces with a high accuracy as is shown in Fig. 20. The time-averaged heat loss per unit mass flow rate in the nozzle  $h_{loss}$  can be evaluated as

$$h_{loss} = \frac{m_n c_{p,n} (T_{\infty} - T_a)}{\dot{m} \Delta t} \quad (18)$$

where  $T_a$  refers to the temperature of the nozzle before the burn.

We modeled the relation between actual thrust coefficient and heat loss in the nozzle assuming that the enthalpy loss of the product gas corresponds to the heat loss  $h_{loss}$  in front of the nozzle. For product gas with a chamber pressure

$p_c$  and the enthalpy  $h_c - h_{loss}$ , quasi-one-dimensional ideal nozzle theory gives evaluations of thrust coefficient and its efficiency in a vacuum as follows:

$$\begin{cases} C_{Fvac} = \frac{F_{vac}}{p_c A_t} = 2 \left\{ \frac{2}{\gamma+1} \left( 1 - \frac{h_{loss}}{h_c} \right) \right\}^{\frac{\gamma}{\gamma-1}} \\ \eta_{C_{Fheat}} \sim \left( 1 - \frac{h_{loss}}{h_c} \right)^{\frac{\gamma}{\gamma-1}} \quad (\text{in vacuum}) \end{cases} \quad (19).$$

$\eta_{C_{Fheat}}$  at sea level was also evaluated in a similar way and varied within  $\pm 3\%$  over the range of the experimental conditions. The reference paper [13] and this evaluation allow us to apply the thrust coefficient  $\eta_{C_F}$  of 0.83 from run #02 to the other experiments.

Figure 21 shows the results of the direct method  $\eta_{c^*}$  and the indirect method  $\eta_{isp}/\eta_{C_F}$  with the error bars of  $1\sigma$  due to uncertainties of measurement systems. As is expected from the numbers of the droplets of melted fuel coming out from the nozzle seen in Fig. 10 a),  $c^*$  efficiency in both the evaluations increased with increasing  $S_e$ . This tendency suggests that the tangential flows produced by swirling injection improved heat transfer, mixing and diffusion of the fuel and oxidizer. However, the direct method seemed to overestimate such effects, giving larger values than the indirect methods due to the large local chamber pressures near the cylindrical wall in the strong swirling flows. Such local pressure effects were reflected in the increasing gap between the two evaluation methods with increasing  $S_e$ . The indirect method seemed to eliminate apparent increase in  $c^*$  efficiency, resulting in lower values than the direct method as expected from similar results in SOFTs using PP [12]. The only exception to this trend is in run #10, but it is not clear that this case, in which the error bar of  $1\sigma$  covers the region where  $\eta_{c^*} > \eta_{isp}/\eta_{C_F}$  as seen in Fig. 21, serves as a counterexample of the trend between the results of the two methods. Therefore, the indirect method has the potential to evaluate the  $c^*$  efficiency of A-SOFTs under various operating conditions without the apparent improvement of performances given that the thrust measurement system is sufficiently accurate.

#### IV. Conclusions

An A-SOFT BBM was developed and a series of static firing experiments was performed as a concept demonstration of a hybrid rocket propulsion system capable of thrust control at a constant O/F using swirling oxidizer injections.

The results of this campaign showed that the A-SOFT BBM demonstrates some of the attributes necessary for the continuous control of thrust at a constant O/F: continuity, monotonicity and predictability of regression rates; and an

O/F and thrust dependent on the two operating variables of oxidizer mass flux and effective geometric swirl number. The model equation proposed in the previous investigations of SOFTs approximated the fuel regression averaged over the burn time and port length to within  $\pm 3.6\%$ . This result suggests that the A-SOFT BBM with axial injection and with positive  $S_e$  larger than 11.0 has the three favorable characteristics of regression rates.

The fuel regression rates averaged over time and port length of the A-SOFT BBM were compared with the fuel regression rates of SOFTs with  $S_g=19.4$  using PP or PMMA. In this comparison, the regression rates of the A-SOFT BBM for  $S_e=25.3$  and  $37.3$  fell within the scatter of the results of the SOFTs with  $S_g=19.4$  due to the decreased performance of the tangential injector of the A-SOFT BBM compared to that of the SOFTs. The regression rate exponents of swirl strength  $n_2$  of the A-SOFT BBM using PP and the SOFTs using PMMA greatly differed, mainly due to the difference in stoichiometric O/Fs of these fuels. The A-SOFT BBM had quite similar axial distributions of regression rates to the SOFTs, though small differences were seen in the tail-end of the fuel port of the A-SOFT BBM. This is probably due to the difference of the port lengths between the tests that were compared.

Other aspects of the A-SOFTs also demonstrated attributes that are favorable for continuous control. The prediction model based on the fuel regression model approximated the time-averaged O/Fs with good accuracy and the polynomial approximation model of thrust also fell within the error bars of the measured thrust. To predict thrust with better accuracy, it is necessary to predict  $c^*$  efficiency under various operating conditions or maintain high  $c^*$  efficiency regardless of operating conditions using baffle plates or post-combustion chambers.

Efforts were made to eliminate positive bias of  $c^*$  efficiency in swirling hybrids using the two methods; in addition to the conventional direct method using actual to ideal chamber pressure ratio  $\eta_{c^*}$ , the indirect method  $\eta_{isp}/\eta_{CF}$  was introduced to eliminate effects of local pressure shift caused by the centrifugal force of swirling flows. In the indirect method,  $\eta_{CF}$  for the axial case run #02 was applied to all other experiments in the campaign because  $C_F$  cannot be evaluated without actual chamber pressure not biased, and depends on the operating conditions over the range tested. Both methods showed the trend of increasing  $c^*$  efficiency with increasing  $S_e$ , but the centrifugal force of swirling flows seemed to enhance the  $c^*$  efficiency of the direct method more than that of the indirect method. This result suggests that the indirect method eliminated the positive bias of  $c^*$  efficiency in the direct method due to centrifugal force in swirling flows. However, large uncertainties in the thrust measurement system decreased the accuracy of the indirect method. With a more accurate thrust measurement system, the indirect method should be able to provide an accurate solution to the  $c^*$  efficiency of A-SOFTs.

This study demonstrated the concept of the A-SOFT hybrid rocket and some of the favorable characteristics for feedback thrust control at a constant O/F, but there are still many challenges remaining before flight demonstrations of A-SOFTs will be practical. Continuous thrust control requires knowledge of hysteresis, uncertainties, stability and transient properties of regression rates and other performances. The practical design of A-SOFTs should involve scaling effects of Reynolds number on fuel regression behavior, like that in SOFT hybrid rockets. The full-development of the boundary layer [15] and forced and free vortices [20] has already been pointed out as representative phenomena dependent on Reynolds number in fluid dynamics in SOFTs, and the similarity found between A-SOFTs and SOFTs implies that these phenomena should lead to scale effects on the fuel regression behavior of A-SOFTs as well. On the other hand, swirling hybrids involve gaseous oxidizer injection for the enhancement of regression rates and combustion stability [14], and this requirement presents another challenge for oxidizer feed systems to have a subsystem vaporizing liquid oxidizer in various throttle rates such as gas generators, catalysts, and regenerative cooling nozzles. Moreover, feedback algorithms to control thrust require a subsystem that senses instantaneous fuel mass flow rate and local port geometry, which should be simple enough to integrate into a light on-board measurement/control subsystem. Multipoint measurements using MIRRAS [21] or ultrasonic sensing systems [22] may satisfy these requirements, but feedback thrust control using these systems had not been demonstrated yet. These research topics on A-SOFTs had been shared and divided in our research community and are currently the subject of ongoing research. Results related to these topics will be revealed in the near future and are expected to have significant impact on the future of hybrid rocket propulsion.

### Appendix A: Evaluation of Uncertainties in Local Regression Rate Measurement

The uncertainty in local regression rate measurements should be discussed to determine the rise in water level  $L$  because these two factors have a trade-off relation with each other. The uncertainty in the measured mass of the water and the rise in water level are assumed as the sources of measurement errors. Uncertainties in port diameter  $r$ , mass of the poured water  $m_w$  and the rise in the water level  $L$ , which are  $\Delta r$ ,  $\Delta L$ , and  $\Delta m_w$ , respectively, have the following relation with one another:

$$\left(\frac{\Delta r}{r_{ref}}\right)^2 = \left(\frac{1}{r_{ref}} \frac{\partial r}{\partial L} \Delta L\right)^2 + \left(\frac{1}{r_{ref}} \frac{\partial r}{\partial m_w} \Delta m_w\right)^2 \quad (20)$$

$$\frac{\Delta r}{r_{ref}} = \frac{1}{2} \sqrt{\left(\frac{\Delta L}{L_{ref}}\right)^2 + \left(\frac{\Delta m_w}{m_{wref}}\right)^2} = \frac{1}{2m_{wref}} \sqrt{(\pi r_{ref}^2 \rho_w \Delta L)^2 + \Delta m_w^2} \quad (21)$$

where  $\rho_w$  refers to the density of the water and the subscript *ref* refers to reference values of the grain and poured water. The uncertainty of  $\rho_w$  was ignored. We should note that the normalized uncertainty  $\Delta r/r_{ref}$  is inversely proportional to  $m_{w_{ref}}$ . The uncertainty of regression rates should be

$$\frac{\Delta \dot{r}}{\dot{r}_{ref}} = \frac{\Delta r}{\dot{r}_{ref} \Delta t} = \frac{r_{ref}}{r_{ref} - r_{0_{ave}}} \frac{1}{2m_{w_{ref}}} \sqrt{(\pi r_{ref}^2 \rho_w \Delta L)^2 + \Delta m_w^2} \quad (22)$$

Where  $r_{0_{ave}}$  refers to the port radius before a burn and its uncertainty was ignored.

The measurement accuracy of the digital scale and the laser distance meter as reported by their manufacturers are 0.1 [g] and 1[mm], respectively. Figure 22 shows the relations among uncertainties of regression rates, rise in water level and water mass poured for  $r_{0_{ave}}=20$  [mm]. To measure 10 to 20 points of the regression rates for the grains with 330[mm] in length,  $m_{w_{ref}}$  from 20 to 30 [g] should be chosen. Figure 22 also shows that this measurement technique gives low accuracy ranging from 0.2 to 0.4 [mm] in  $1\sigma$ . To improve the measurement accuracy, the use of a more accurate laser distance meter has the largest impact. For example, a laser distance meter with a 0.1 [mm] accuracy enables the measurement of 2 [mm] of fuel regression for 5 [s] at a 20 [mm] rise in water level with an accuracy of 0.03 [mm/s] in regression rate whereas a digital scale with 0.01[g] in accuracy hardly improves measurement accuracy of regression rates.

### Acknowledgments

This research was supported by the Hybrid Rocket Research Working Group (HRrWG) of the Institute of Space and Astronautical Science, Japan Aerospace Exploration Agency. The authors thank members of HRrWG for their helpful discussion. The authors thank the members of HRrWG for their helpful advice, discussion and assistance conducting firing experiments.

This work was also financially supported by JSPS KAKENHI 15J08028.

The authors express appreciation for the collaboration in firing experiments of Prof. Yasuhiro TANI and Mr. Kazuhiko MORISHITA in Kyushu University, and thank the undergraduate and graduate students at Kyushu University, Mr. Masato YAMASHITA, Mr. Masato MIZUCHI, Mr. Koki KATAKAMI and Mr. Yudai MAJI, for great help in the building and operation of the firing test facility.

The authors also thank Prof. Yutaka WADA of Chiba Institute of Technology for the significant help and advice on the building and operation of the experimental setup.

Finally, the authors especially thank the graduate students at ISAS/JAXA, Mr. Tomoaki USUKI and Mr. Genki MISHIMA for the great help from the start of this project to the experiments at Kyushu University.

## References

- [1] Waidmann, W., "Thrust Modulation in Hybrid Rocket Engines," *Journal of Propulsion and Power*, Vol. 4, No. 5, 1988, pp. 421-427.  
doi: 10.2514/3.23083
- [2] Ozawa, K., and Shimada, T., "Effects of O/F Shifts on Flight Performances of Vertically Launched Hybrid Sounding Rockets," *53rd AIAA/SAE/ASEE Joint Propulsion Conference*, AIAA, Atlanta, Georgia, 2017, AIAA 2017-5051.  
doi: 10.2514/6.2017-5051
- [3] Usuki, T., and Shimada, T., "Improvement on Thrust Profile Flexibility by Oxidizer-to-Fuel Ratio Feedback Control in Hybrid Rocket," *66th International Astronautical Congress*, IAF, Jerusalem, Israel, IAC-15, C4, 2, 3, 2015.
- [4] Yuasa, S., and Kitagawa, K., "Current Status of Rocket Developments in Universities," *The Journal of Space Technology and Science*, Vol. 21, 2005, p. 1\_1-1\_11.  
doi: 10.11230/jsts.21.1\_1
- [5] Knuth, W. H., Chiaverini, M. J., Sauer, J. A., and Gramer, D. J., "Solid-Fuel Regression Rate Behavior of Vortex Hybrid Rocket Engines," *Journal of Propulsion and Power*, Vol. 18, No. 3, 2002, pp. 600-609.  
doi:10.2514/2.5974
- [6] Tamura, T., Yuasa, S., and Yamamoto, K., "Effects of Swirling Oxidizer Flow on Fuel Regression Rate of Hybrid Rockets," *35th AIAA/ASME/SAE/ASEE Joint Propulsion Conference & Exhibit*, AIAA, Los Angeles, California, 1999, AIAA 99-2323.  
doi: 10.2514/6.1999-2323
- [7] Shimada, T., Yuasa, S., Nagata, H., Aso, S., Nakagawa, I., Sawada, K., Hori, K., Kanazaki, M., Chiba, K., Sakurai, T., Morita, T., Kitagawa, K., Wada, Y., Nakata, D., Motoe, M., Funami, Y., Ozawa, K., Usuki, T., "Hybrid Propulsion Technology Development in Japan for Economic Space Launch," edited by L. De Luca, T. Shimada, V. P., Sinditskii, and M. Calabro, *Chemical Rocket Propulsion: A Comprehensive Survey of Energetic Materials*, Springer Aerospace Technology, Springer International Publishing, Cham, Switzerland, 2017, pp. 545-575.  
doi: 10.1007/978-3-319-27748-6
- [8] Blume, A. P., *LabVIEW Style Book*, The National Instruments Virtual Instrumentation, Prentice Hall, New Jersey, 2007.
- [9] Marxman, G. A., Wooldridge, C. E., and Muzzy, R. J., "Fundamentals of Hybrid Boundary Layer Combustion," *Heterogeneous Combustion Conference*, edited by H. G. Wolfhard, I. Glassman, and L. Green, Jr., Vol. 15, AIAA Progress in Astronautics and Aeronautics, Academic Press, New York, 1964, pp. 485-521.

doi: 10.2514/6.1963-505

- [10] Lengellé, G., "Solid-Fuel Pyrolysis Phenomena and Regression Rate, Part 1: Mechanisms," *Fundamentals of Hybrid Rocket Combustion and Propulsion*, edited by M. J. Chaiverini, and K. K. Kuo, Progress in Astronautics and Aeronautics, AIAA, Reston, VA, 2007, pp. 93-121.
- doi: 10.2514/4.866876
- [11] Gordon, S., and McBride, J. B., "Computer Program for Calculation of Complex Chemical Equilibrium Compositions and Applications," NASA Reference Publication 1311, 1994.
- [12] Yuasa, S., Shiraishi, N., Sakamoto, M., Sezaki, C., Hirata, K., and Sakurai, T., "Evaluation Method of C\* Efficiency of Swirling-Oxidizer-Flow-Type Hybrid Rocket Engines," *Journal of the Japan Society for Aeronautical and Space Sciences*, Vol. 59, No. 687, 2011, pp. 97-101. (Japanese)
- doi: 10.2322/jjsass.59.97
- [13] "Sonic Nozzles for Mass Flow Measurement and Reference Nozzles for Thrust Verification," AGARD Advisory Report 321, 1997.
- [14] Pucci, J. M., "The Effects of Swirl Injector Design on Hybrid Flame-Holding Combustion Instability," *38th AIAA/ASME/SAE/ASEE Joint Propulsion Conference & Exhibit*, AIAA, Indianapolis, Indiana, 2002, AIAA 2002-3578.
- doi : 10.2514/6.2002-3578
- [15] Ozawa, K., and Shimada, T., "A Linear Stability Analysis of Unique Low Frequency Mode on Uni-directional Vortex Injection Hybrid Rocket Engines," *65th International Astronautical Congress*, IAF, Toronto, Canada, IAC-14, C4, 5, 7, 2014.
- [16] Development of Scalable Space-Time Averaged Regression Rate Expressions for Hybrid Rockets  
Karabeyoglu, M. A., Cantwell, B. J., Greg Zilliac, " ," *Journal of Propulsion and Power*, 2007, Vol.23: 737-747,  
10.2514/1.19226
- [17] Shiraishi, N., and Yuasa, S., "Prediction Method of Time Variation of Swirling-Oxidizer-Flow-Type Hybrid Rocket Engine Performance Based on Local Fuel Regression Rates," *Journal of the Japan Society for Aeronautical and Space Sciences*, Vol. 61, No. 3, 2013, pp. 71-78. (Japanese)
- doi: 10.2322/jjsass.61.71
- [18] Saito, D., Yuasa, S., and Sakurai, T., "Three Dimensional Visualization of Flames in Combustion Chamber of Swirling-Oxidizer-Flow-Type Hybrid Rocket Engine," *Proceedings of the 53rd Conference on Aerospace Propulsion and Power*, Kurashiki, Okayama, Japan, JSASS, 2013, JSASS-2013-0025. (Japanese)
- [19] Carslaw, H., S., and Jaeger, J., C., *Conduction of Heat in Solids*, 2nd ed., Oxford University Press, Oxford, 1959, Chap. 7. 4.
- [20] Majdalani, J., "Vortex Injection Hybrid Rockets," *Fundamentals of Hybrid Rocket Combustion and Propulsion*, edited by M. J. Chaiverini, and K. K. Kuo, Progress in Astronautics and Aeronautics, AIAA, Reston, VA, 2007, pp. 247-276.

doi: 10.2514/4.866876

- [21] Gramer, D. J., Taagen, T. T., Vermaak, A. G., Harris, J. D., Peissig, D. E., Evans, B. J., Selig, C. J., Mitten, M., and Chiaverini, M. J., "Final Report on Miniature Resistive Regression and Ablation Sensor," OTC-GS-0073-FR-2001-1, Orbital Technologies Corp., NASA Small Business Innovative Research Phase II Rep., Madison, WI, Jan. 2001
- [22] Cauty, F., Serýn, N., Gramer, D., "Solid-Fuel Pyrolysis Phenomena and Regression Rate, Part 2: Measurement Techniques," *Fundamentals of Hybrid Rocket Combustion and Propulsion*, edited by M. J. Chaiverini, and K. K. Kuo, Progress in Astronautics and Aeronautics, AIAA, Reston, VA, 2007, pp. 167-318.

doi: 10.2514/4.866876

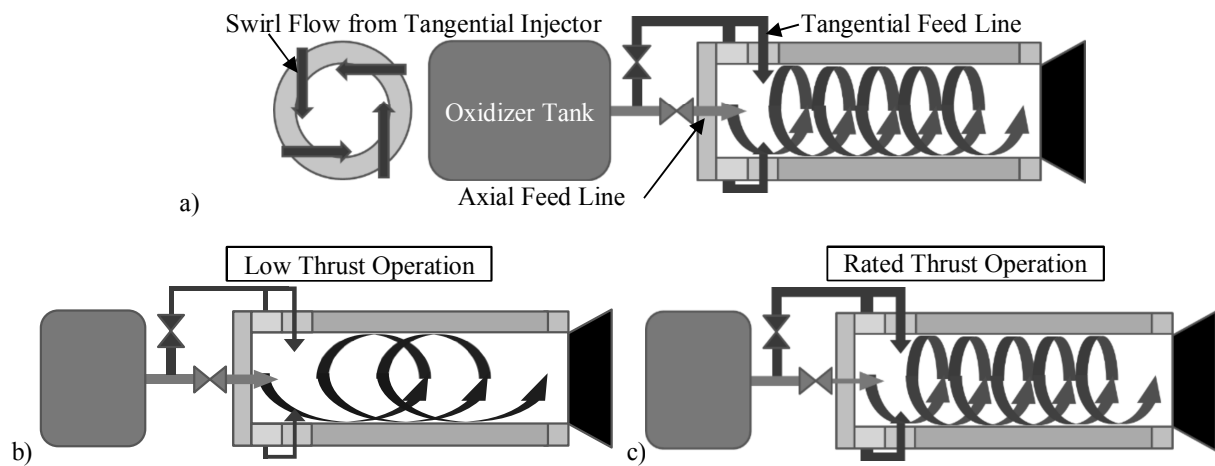


**Fig. 1 a) Concept of Altering-intensity Swirling-Oxidizer-Flow-Type (A-SOFT) hybrid rocket engines. b) Small thrust operation of A-SOFTs for a constant O/F. c) Large thrust operation of A-SOFTs for a constant O/F.**

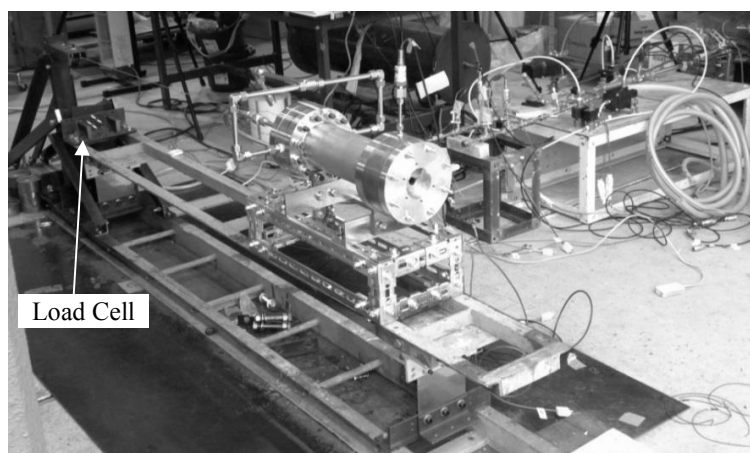


**Fig. 2 Experimental setup of the A-SOFT BBM.**

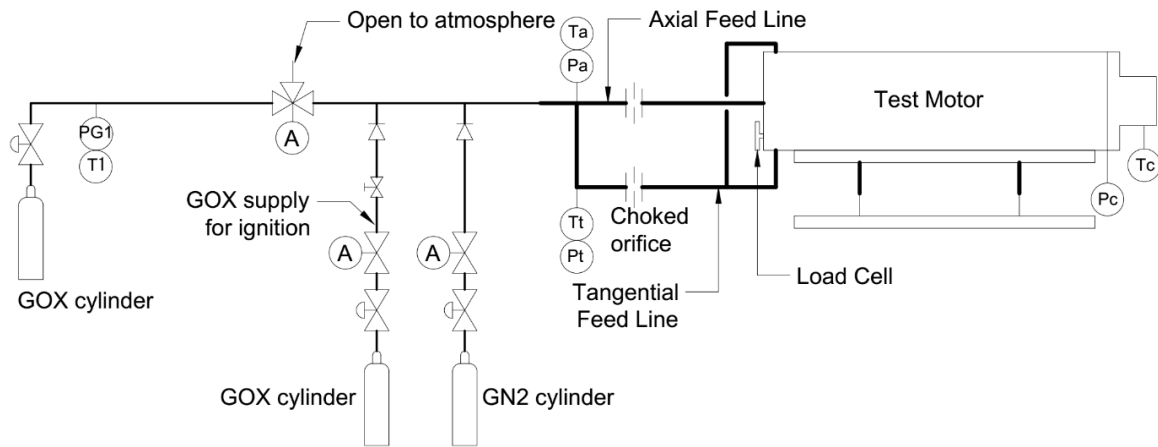


Fig. 3 Schematic of the feed system, control and sensing devices, and engine.

Table 1 List of the choked orifices used in the firing experiments

Diameter, mm	Discharge Coefficient	Accuracy of Discharge Coefficient ( $1\sigma$ ), $\times 10^4$
2.6	0.885	18.2
2.4	0.872	8.30
2.2	0.876	9.88
1.3	0.762	31.2

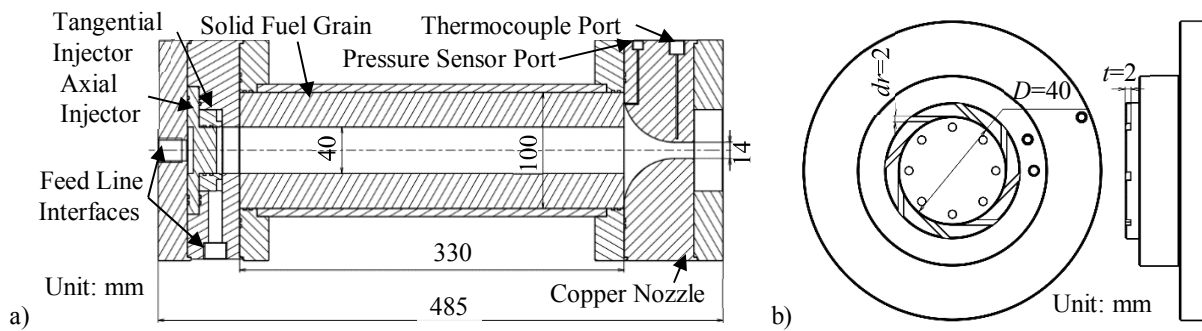
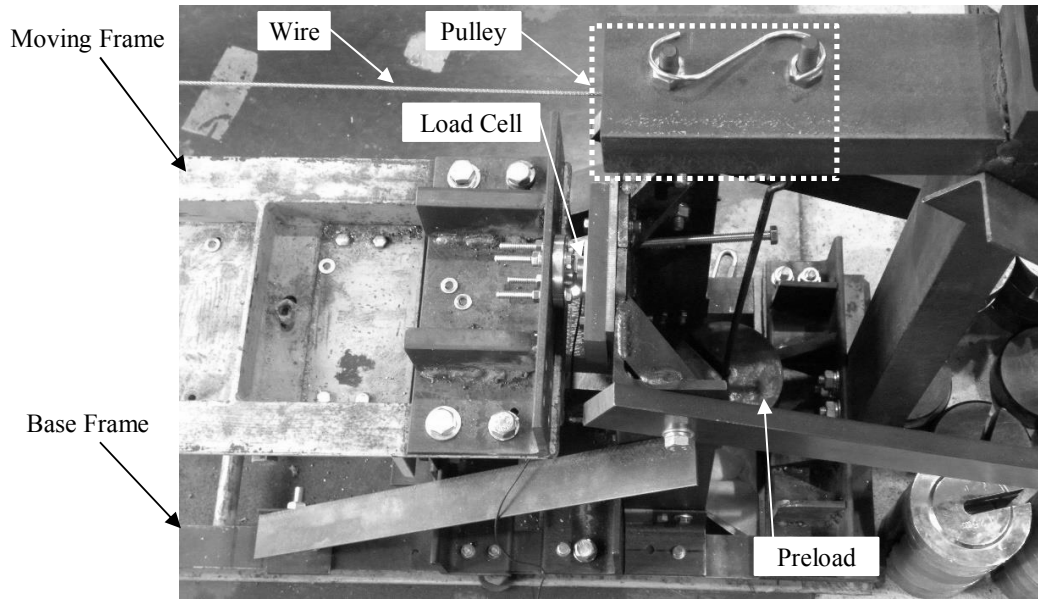


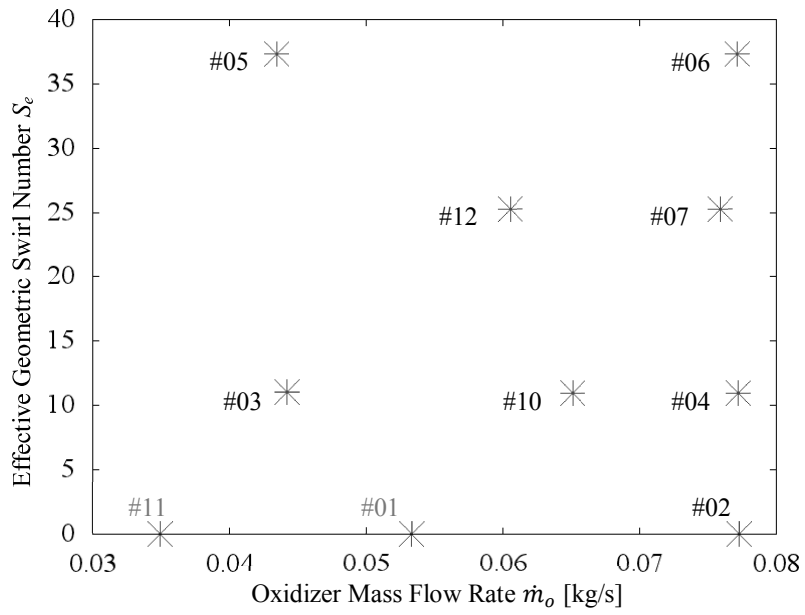
Fig. 4 a) Cross-section of the A-SOFT BBM. b) Design of the dual injector assembly.



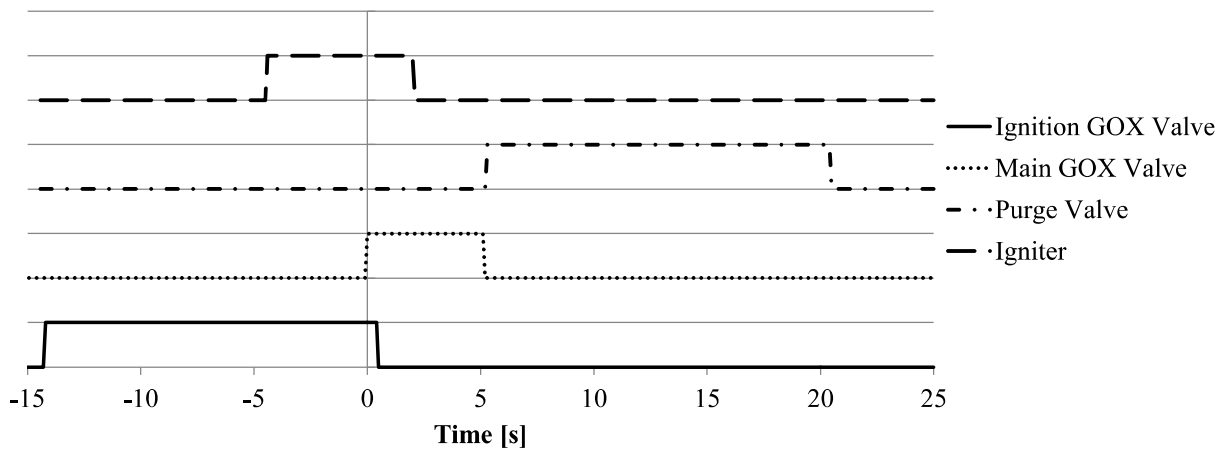
**Fig. 5** Close view of the thrust measuring system around the load cell and the preload.

**Table 2** Experimental conditions in the static firing experiments of the A-SOFT BBM

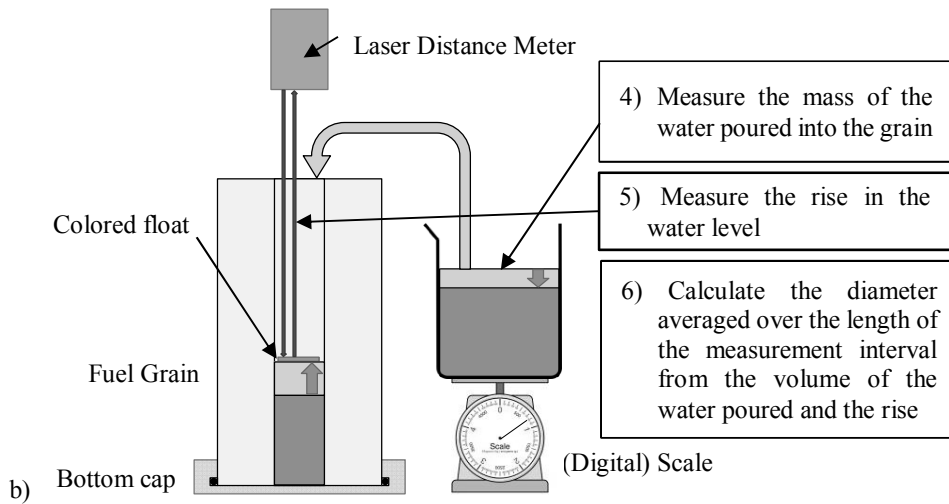
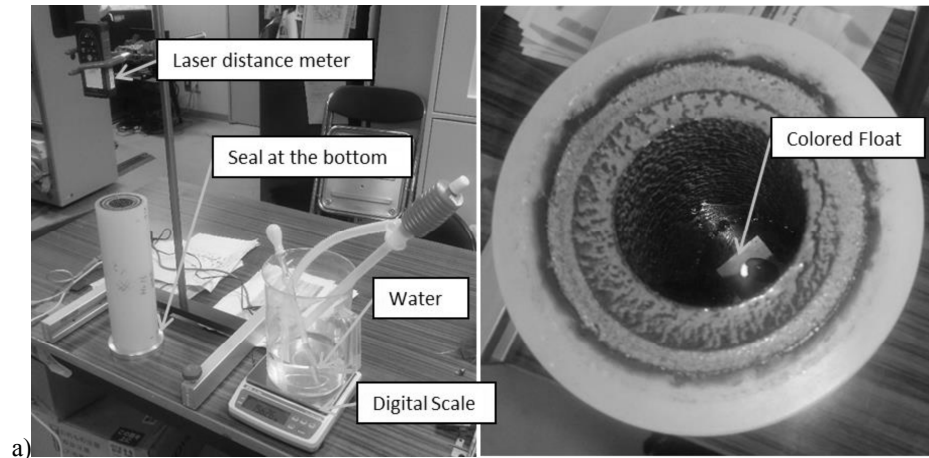
Run, No.	Target GOX Mass Flow Rate, g/s	Target $S_e$	Axial Feed Line Orifice DIA, mm	Tangential Feed Line Orifice DIA, mm	Expected Thrust, N	Expected Chamber Pressure, MPa	Nominal Burn Time, s
#01	54.8	0.0	2.6	0	104	0.62	5.0
#02	78.3	0.0	2.6	0	147	0.85	5.0
#03	41.9	11.0	2.2	2.4	106	0.64	5.0
#04	78.3	11.0	2.2	2.4	191	1.08	5.0
#05	41.9	37.3	0	2.6	114	0.67	5.0
#06	78.3	37.3	0	2.6	226	1.26	5.0
#07	78.3	25.3	1.3	2.6	214	1.20	5.0
#08	41.9	25.3	1.3	2.6	115	0.68	5.0
#09	41.9	25.3	1.3	2.6	115	0.68	5.0
#10	61.1	11.0	2.2	2.4	152	0.88	5.0
#11	41.9	0.0	2.6	0	78.8	0.49	5.0
#12	61.1	25.3	1.3	2.6	169	0.96	5.0



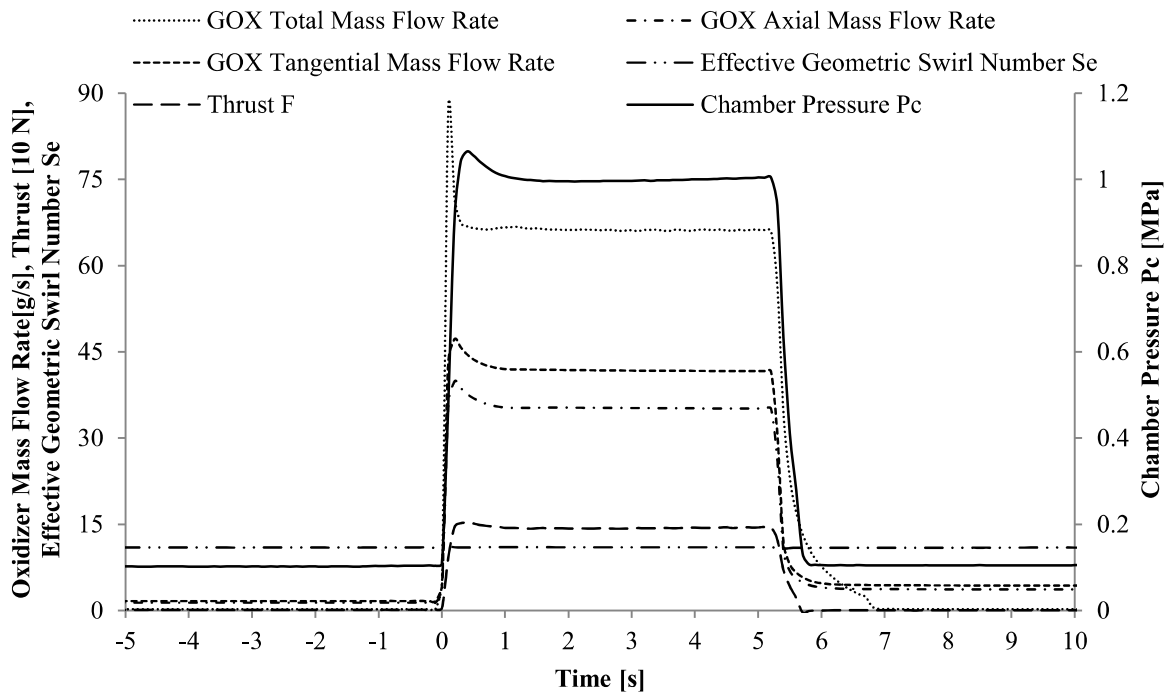
**Fig. 6 Summary of the experimental conditions in the firing experiments.**



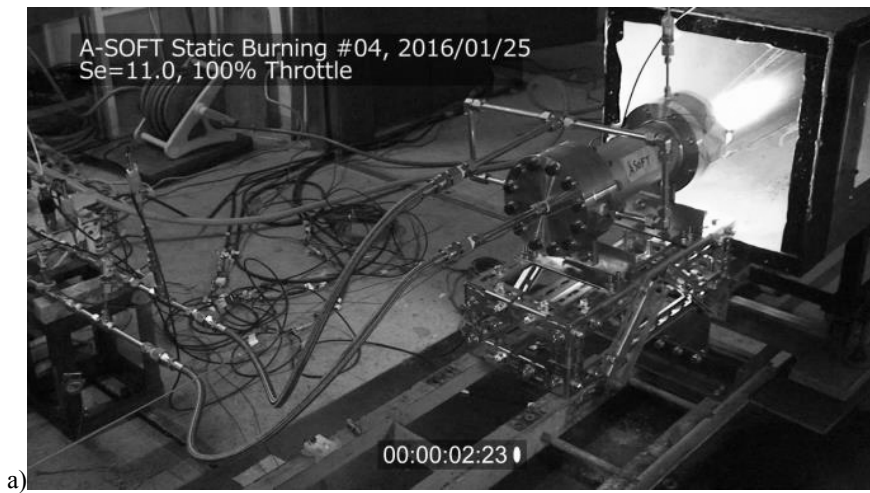
**Fig. 7 Time sequence of an A-SOFT BBM static firing experiments.**



**Fig. 8 Measurement system for axial distribution of regression rates. a) Measurement setup b) Measurement procedure of local fuel port diameter after a burn.**



**Fig. 9** Typical time traces of the A-SOFT BBM static firing experiments for 100% throttle rate and  $S_e = 11.0$  (run #04).



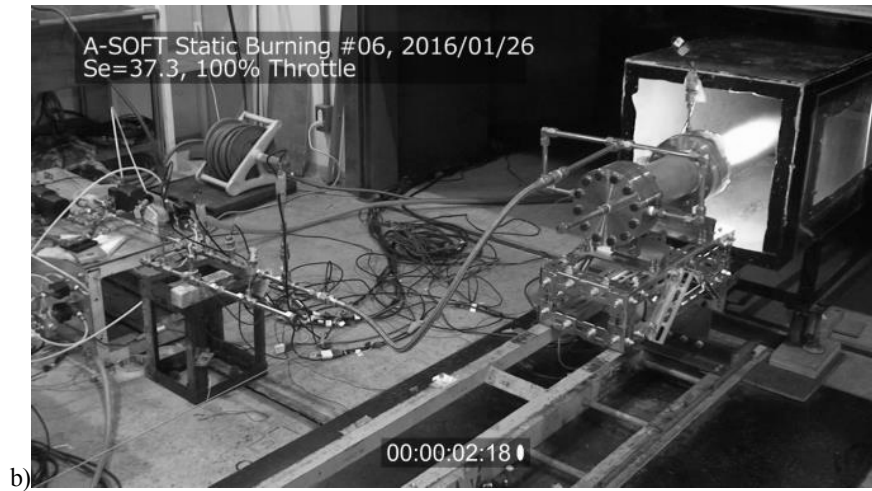


**Fig. 10** Typical views of static firing experiments of the A-SOFT BBM. a) 100% throttle,  $S_e=11.0$  (run #04). b) 100% throttle,  $S_e=37.3$  (run #06).

**Table 3** Summary of the firing experiments of the A-SOFT BBM. The density of the grain for the run #01 is estimated from those of the other grains for the lack of data, and the inner diameter and the other ideal performance data for the run #01, which were marked with “\*”, was calculated from the estimated density.

Run No.	Init. Condition of Fuel			Inner DIA		Fuel Mass		Burn Time	GOX Mass Flow Rate	$S_e$
	Length	Outer DIA	Density	Initial	End	Initial	End			
	mm	mm	kg/m <sup>3</sup>	mm	mm	kg	kg	s	g/s	-
#01	329.65	99.79	905.9	39.95*	40.75*	1961.1	1945.8	1.9	53.30	0.00
#02	329.55	99.75	904.5	40.03	43.64	1954.4	1883.5	5.2	77.26	0.00
#03	329.55	99.75	904.7	40.05	44.19	1954.1	1872.4	5.2	44.18	11.00
#04	329.60	99.75	905.5	40.04	45.54	1956.6	1846.3	5.2	77.20	10.97
#05	329.65	99.72	904.9	40.05	44.98	1953.8	1855.5	5.2	43.39	37.30
#06	329.55	99.70	904.9	40.07	47.11	1952.2	1808.4	5.2	77.12	37.30
#07	329.65	99.75	911.1	40.06	46.49	1968.6	1837.3	5.2	75.91	25.31
#10	329.60	99.75	905.2	40.26	45.18	1951.8	1853.3	5.2	65.15	10.98
#11	329.55	99.75	905.9	40.20	41.45	1954.0	1930.1	5.2	34.87	0.00
#12	329.50	99.75	906.4	40.03	45.53	1958.1	1847.8	5.2	60.51	25.30

Run No.	Reg-rate	O/F	Pressure		Thrust		$c^*$	$I_{sp}$	$\eta_{c^*}$	$\eta_{I_{sp}}/\eta_{C_F}$
			Real	Ideal	Real	Ideal				
	mm/s	-	MPa	MPa	N	N	m/s	s	-	-
#01	0.21*	6.62*	0.51	0.57*	50.1	93.3*	1425.1	155.1	0.89	0.55
#02	0.36	5.67	0.79	0.87	113.7	151.1	1474.0	169.6	0.91	0.76
#03	0.42	2.81	0.62	0.64	87.3	107.1	1644.6	182.4	0.96	0.82
#04	0.56	3.64	1.00	1.02	142.7	179.6	1594.3	186.1	0.98	0.80
#05	0.50	2.30	0.69	0.68	93.2	114.3	1673.2	187.2	1.01	0.81
#06	0.74	2.79	1.16	1.13	166.7	200.9	1660.5	195.6	1.02	0.83
#07	0.67	3.01	1.03	1.08	148.4	191.2	1643.1	192.8	0.96	0.78
#10	0.50	3.44	0.87	0.88	124.4	152.4	1605.1	184.8	1.00	0.82

#11	0.12	7.59	0.28	0.35	31.2	52.4	1381.6	135.5	0.79	0.65
#12	0.56	2.85	0.84	0.88	118.8	152.2	1649.4	189.9	0.96	0.78

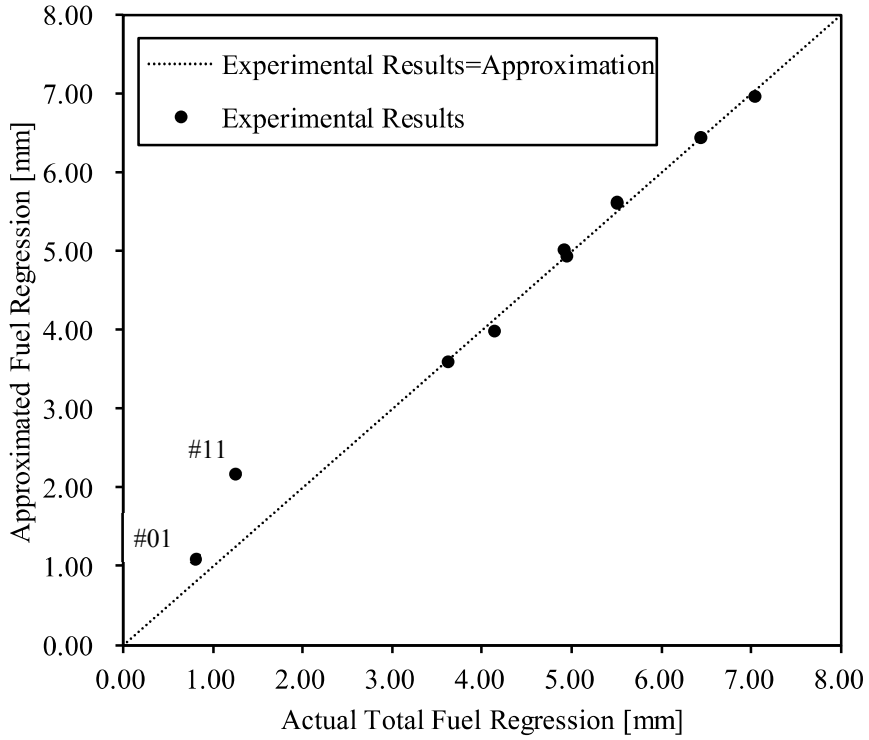


Fig. 11 Comparison of fuel regression between the experimental data and the approximated model Eq. (3).

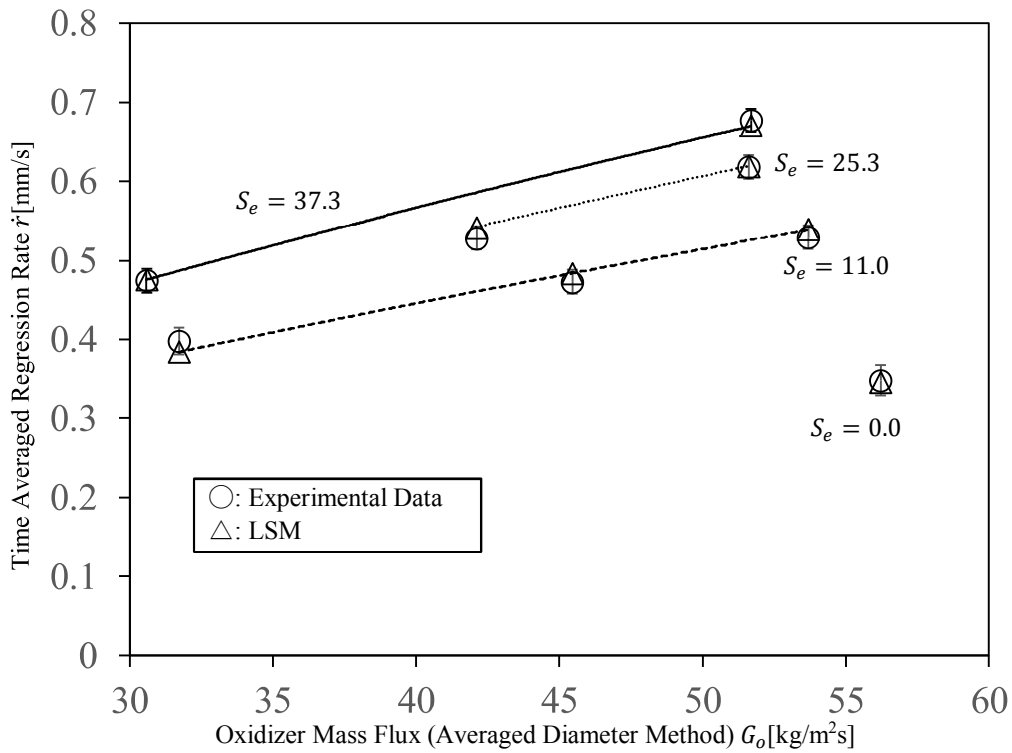
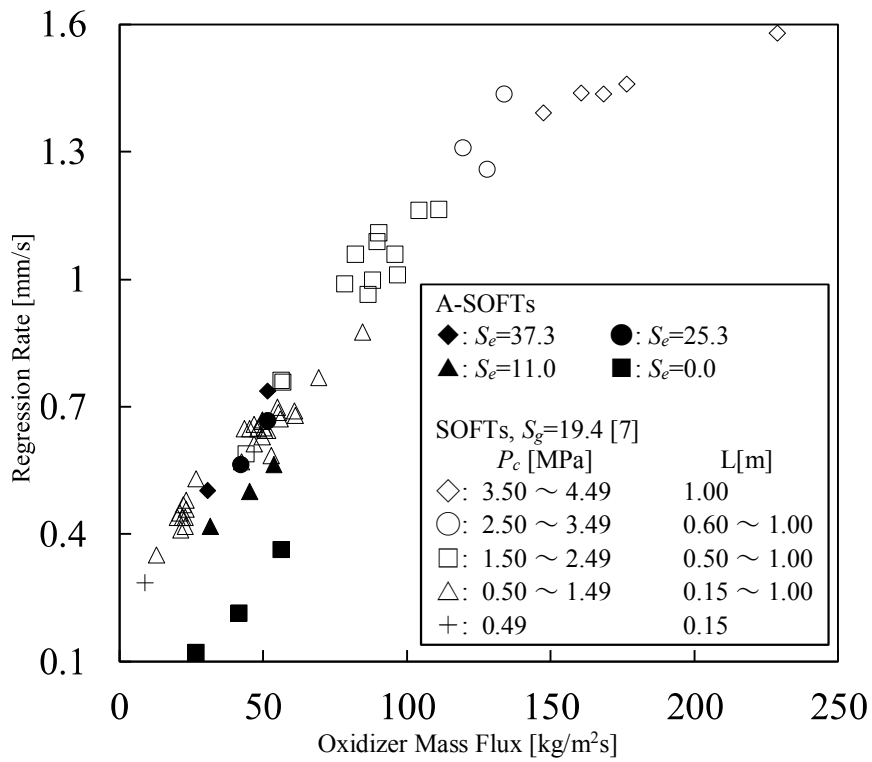
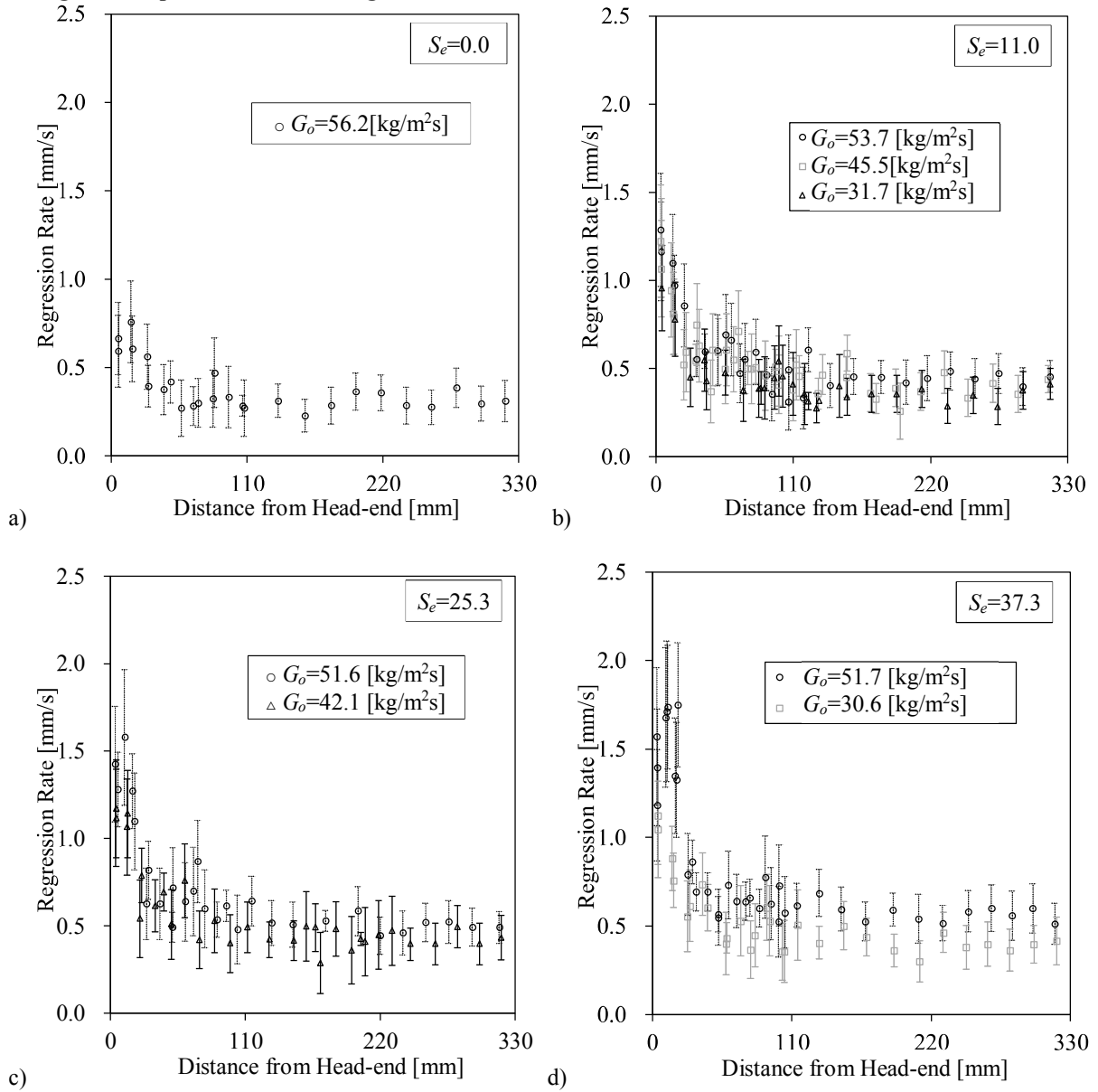


Fig. 12 Averaged regression rates of the A-SOFT BBM and their multiple linear regression using Eq. (3).



**Fig. 13 Comparison of the fuel regression rates between the A-SOFT BBM and the SOFTs with  $S_g=19.4$ .**



**Fig. 14 Comparison of the axial distributions of the regression rates for various oxidizer mass flow rate and effective geometric swirl number.**

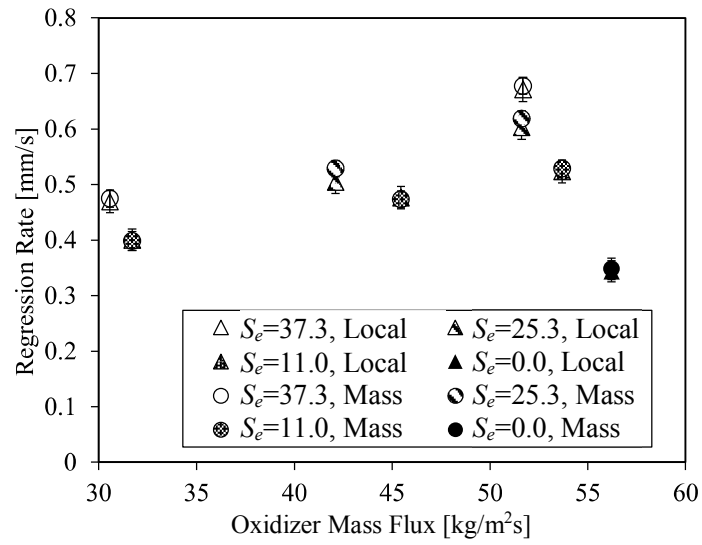


Fig. 15 Comparison of the results of the two measurement methods of the regression rates averaged over the port length and the burn time. “Local” refers to regression rates based on the results of axial distribution of regression rates, and “Mass” refers to those calculated from decrease of masses of solid fuel grain.

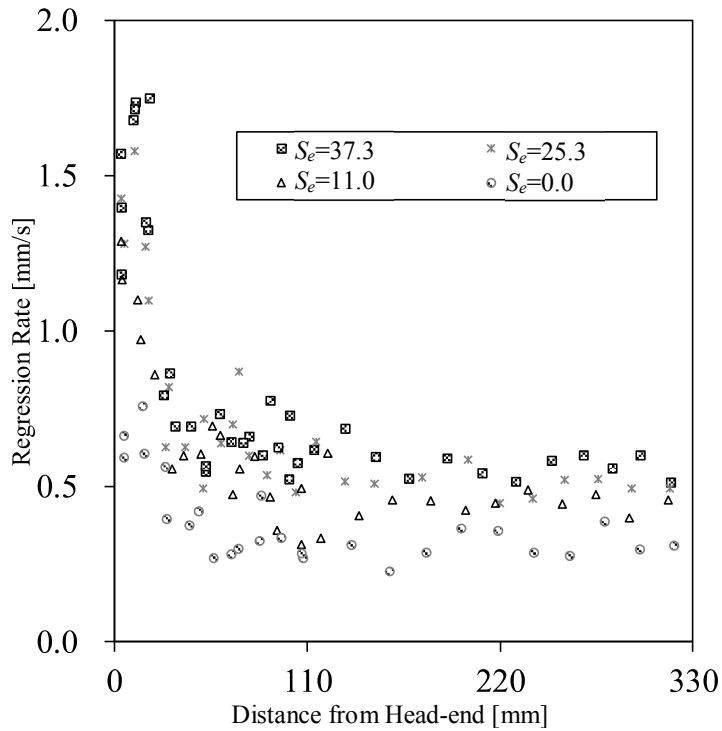


Fig. 16 Comparison of the axial distribution of the regression rates of the A-SOFT BBM for various effective geometric swirl number and 100% throttle rate.

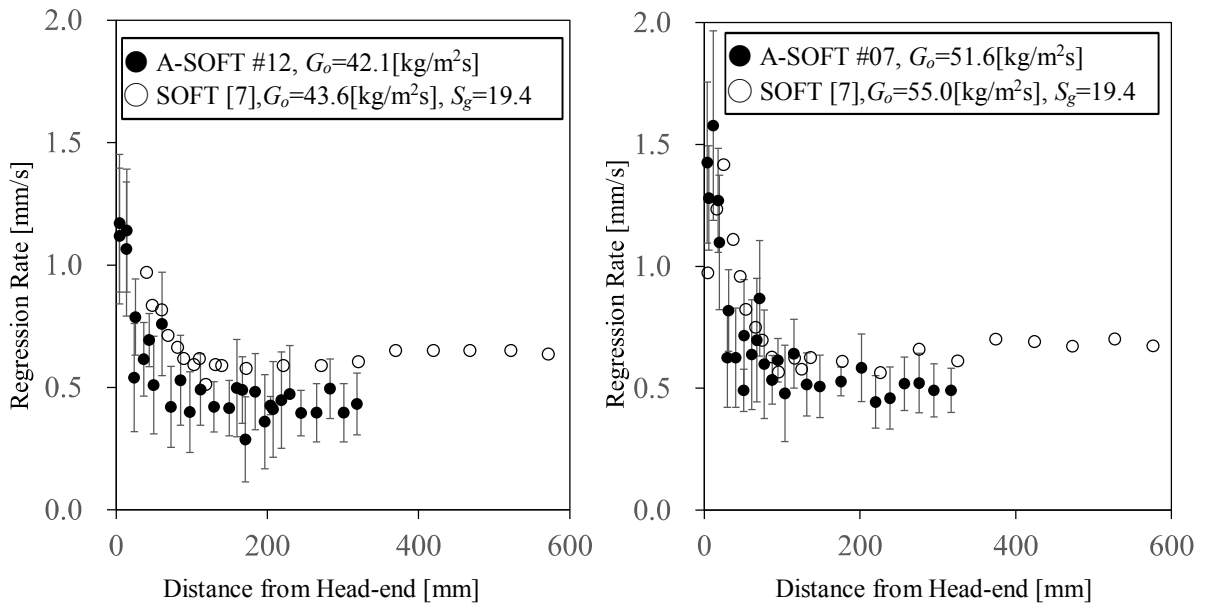


Fig. 17 Comparison of the axial distributions of the regression rates between the A-SOFT BBM and the SOFTs

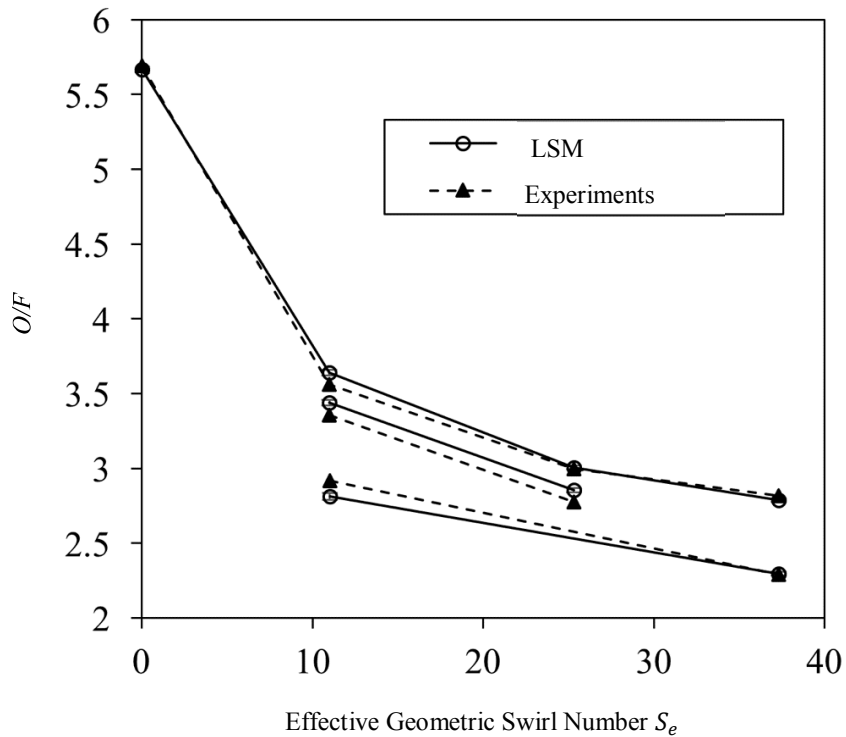


Fig. 18 Relations between the time-averaged O/F and  $S_e$  of the A-SOFT BBM.

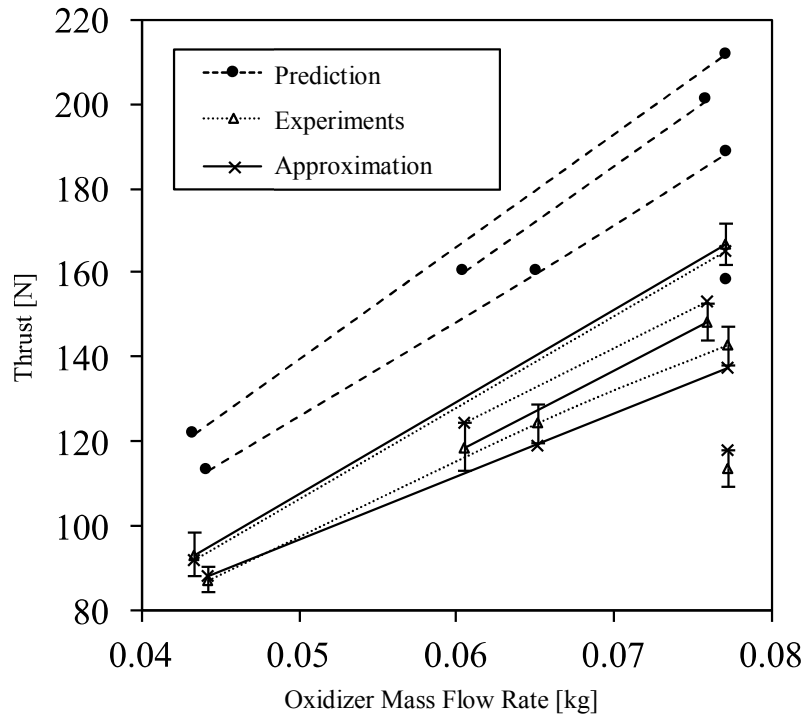


Fig. 19 Comparison among the predicted, measured, and approximated thrust of the A-SOFT BBM.

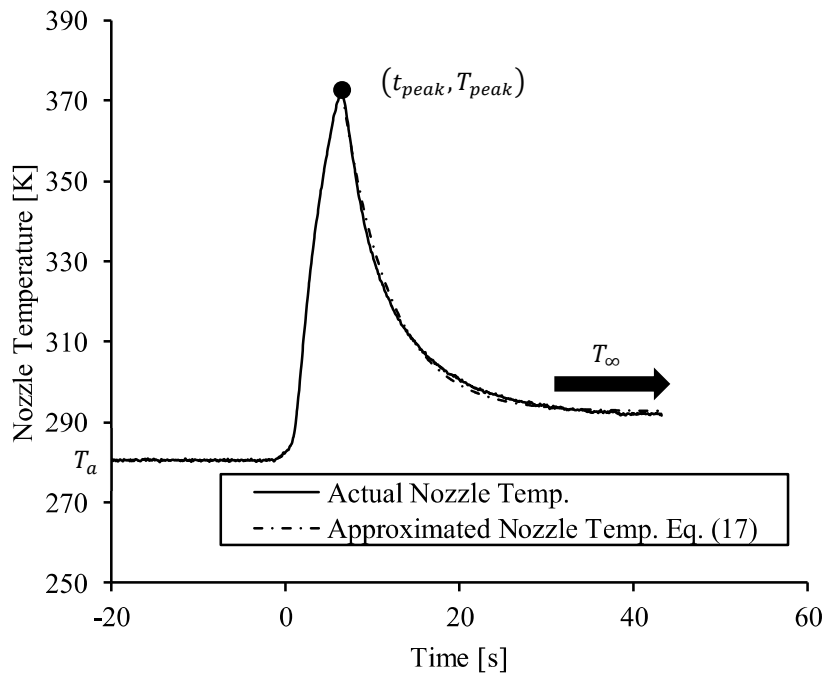


Fig. 20 Comparison between the temperature in the copper nozzle and the approximation Eq. (17) for the run #02.

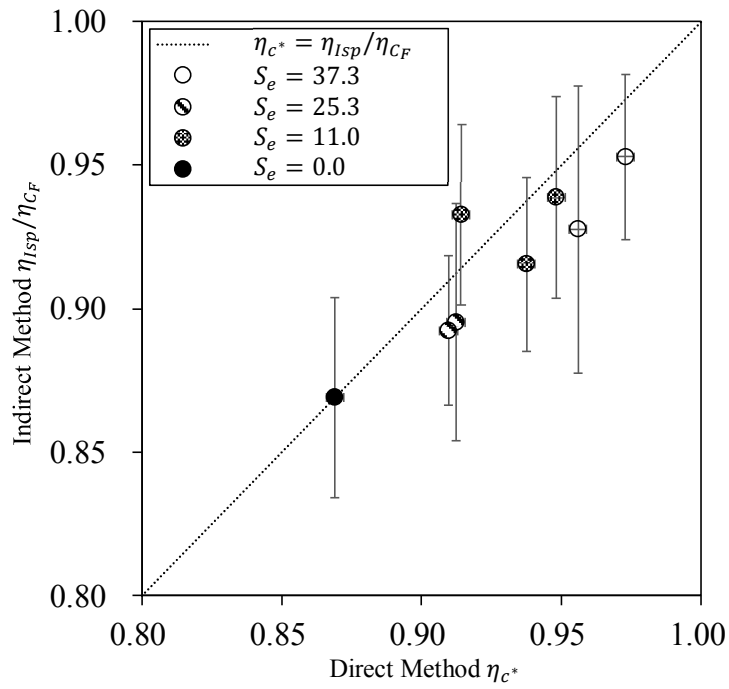


Fig. 21 Relations between  $\eta_{c^*}$  and  $\eta_{isp}/\eta_{cF}$  of the A-SOFT BBM.

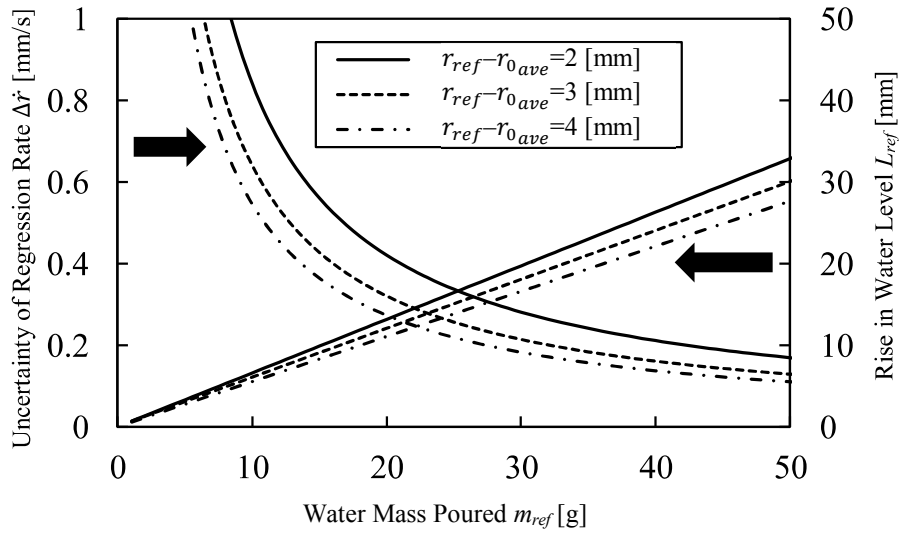


Fig. 22 Relation between the expected measurement accuracy and measurement pitch in the local regression rate measurement.